

The Effect of Non-Gaussian Noise on Auto-correlative Weak-value Amplification

Jing-Hui Huang^{1,2,*}, J. S. Lundeen^{2,†}, Adetunmise C. Dada^{3,‡}, Kyle M.

Jordan^{2,§}, Guang-Jun Wang^{4,¶}, Xue-Ying Duan⁴, and Xiang-Yun Hu^{1,**}

¹*Institute of Geophysics and Geomatics, China University of Geosciences, Lumo Road 388, 430074 Wuhan, China.*

²*Department of Physics and Centre for Research in Photonics,*

University of Ottawa, 25 Templeton Street, Ottawa, Ontario, Canada K1N 6N5

³*School of Physics and Astronomy, University of Glasgow, Glasgow G12 8QQ, UK and*

⁴*School of Automation, China University of Geosciences, Lumo Road 388, 430074 Wuhan, China.*

Accurate knowledge of the spectral features of noise and their influence on open quantum systems is fundamental for quantitative understanding and prediction of the dynamics in a realistic environment. For the weak measurements of two-level systems, the weak value obtained from experiments will inevitably be affected by the noise of the environment. Following our earlier work on the technique of the auto-correlative weak-value amplification (AWVA) approach under a Gaussian noise environment, here we study the effect of non-Gaussian noise on the AWVA technique. In particular, two types of noise with a negative-dB signal-to-noise ratio, frequency-stationary noises and frequency-nonstationary noises are studied. The various frequency-stationary noises, including low-frequency ($1/f$) noises, medium-frequency noises, and high-frequency noises, are generated in Simulink by translating the Gaussian white noise with different band-pass filters. While impulsive noise is studied as an example of frequency-non stationary noises. Our simulated results demonstrate that $1/f$ noises and impulsive noises have greater disturbance on the AWVA measurements. In addition, adding one kind of frequency-stationary noise, clamping the detected signals, and dominating the measurement range may have the potential to improve the precision of the AWVA technique with both a smaller deviation of the mean value and a smaller error bar in the presence of many hostile non-Gaussian noises.

I. INTRODUCTION

Precise replication and characterization of the noise influencing a non-isolated system of interest have far-reaching implications across a variety of areas of physics, such as quantum measurement [1–5], quantum information processing [6–8], and the hot topic of identifying weak signals in gravitational wave astronomy [9–13]. These measurements cannot be isolated from the surrounding environment and are usually influenced by the technical noise. Particularly, for the quantum dynamics of two-level systems, the environment described by Josephson junctions [14] or Cooper pair boxes [15] was normally considered using low-frequency noise sources with the non-Gaussian distribution. Recently, the quantum weak measurement of two-level systems derived by Aharonov, Albert and Vaidman in 1988 [16] has attracted special attention in amplification of signals that are small above technical background noise, direct quantum state and geometric phase determination, and observation of nonclassical features of quantum mechanics [17–22].

In principle, choosing nearly orthogonal pre-selected and post-selected states leads to a *weak value*, which may lie outside of the eigenvalue spectrum of a standard projective measurement. This feature, known as

the weak-value amplification (WVA) technique, has led to great achievements in the estimation of unknown small physical quantities, such as velocities [23, 24], angular rotation shifts [25, 26], frequency shifts [27, 28], the weak magnetic fields detection [29]. Although increasing the orthogonality decreases the probability of detecting photons and makes the weak measurement difficult with a lower signal-to-noise ratio (SNR), an increasing number of experiments and theories have demonstrated the WVA technique [30–32] and its modifications [19, 24, 33–37] outperform the conventional optical interference scheme in the presence of the certain technical limits. Further, the effect of technical noise and the surrounding environment on the WVA technique [38–42] has been investigated recently. In particular, WVA under random telegraph noise and non-Gaussian (colored) noises are discussed in Ref. [3], where it was shown that large weak value can be obtained due to the memory effect of the non-Markovian environment. Therefore, the influence of non-Gaussian noises on the WVA technique and its modifications is worth studying.

Our earlier work on the auto-correlative weak-value amplification (AWVA) technique under strong Gaussian white noise background demonstrated that the AWVA technique outperforms the standard WVA technique in the time domain with smaller statistical errors [43]. Nevertheless, Gaussian white noise has been replaced by non-Gaussian noise in a variety of areas of physics [44–47]. Particularly, characterization of the LIGO detectors via investigations of noise types (even including transient non-Gaussian noise) that most impact the astrophysical searches and mitigation of noise couplings will con-

* Email: jinghuihuang@cug.edu.cn

† Email: jeff.lundeen@gmail.com

‡ Email: Adetunmise.Dada@glasgow.ac.uk

§ Email: kjordan@uottawa.ca

¶ Email: gjwang@cug.edu.cn

** Email: xyhu@cug.edu.cn

tinue to play a critical role in gravitational-wave astronomy [9–12]. Note that the scheme of the AWVA technique is similar to that used for measuring phase shifts in gravitational wave detection. Here, we further numerically investigate the influence of non-Gaussian noise on the AWVA technique with a negative-dB SNR. The various types of non-Gaussian noises are generated in Simulink by translating the Gaussian white noise with different band-pass filters. Then, the sensitivity of the auto-correlative intensity Θ under various non-Gaussian noises is calculated and the effect of the noises on the AWVA technique is discussed.

The paper is organized as follows. In Sec II A we briefly introduce the auto-correlative weak-value amplification technique for measuring a time delay τ , and introduce the auto-correlative intensity Θ to evaluate the weak value. In Sec II B we present the white noise, the various types of non-Gaussian noises, and their properties. In Sec III we show the results on Simulink under various types of noises and propose effective techniques for enhancing the precision of the AWVA measurements under the worst cases. Finally, Sec IV is devoted to a summary of the results and discussions.

II. THE AWVA TECHNIQUE UNDER NON-GAUSSIAN NOISES

A. The AWVA technique with auto-correlative intensity

We briefly review the auto-correlative weak-value amplification (AWVA) approach of Ref. [43] for estimating a time delay τ induced by a birefringent crystal. The scheme is shown in Fig. 1, which corresponds to a two-level system in a quantum state $|\Phi\rangle$ and a measurement device represented by a temporal pointer $|\Psi\rangle$. The standard WVA technique [30–32] is shown in the red box without a 50:50 beam splitter (BS) in Fig 1. Note that the main difference between the WVA technique and the AWVA technique is that an additional light path is added in the AWVA scheme, by dividing the light after pre-selection into two light paths with BS. In one path, light passes through the birefringent crystal and P2 as in the WVA scheme, while in the other path light passes only through polarizer 3 (P3) for an auto-correlative measurement.

Similarly, the AWVA technique includes an initial preparation of the measured system $|\Phi_i\rangle$ and the pointer $|\Psi_i\rangle$, weak interaction between the system and the pointer, a post-selection on the system via projection on state $|\Phi_f\rangle$ and a projective measurement on the pointer $|\Psi_{f1}\rangle$, the same projective measurement on the pointer $|\Psi_{f2}\rangle$ without the weak interaction, and finally, determination of the auto-correlative intensity Θ between the outcomes of the pointers $|\langle\Phi_{f1}|\Phi_i\rangle|^2$ and $|\langle\Phi_{f2}|\Phi_i\rangle|^2$. To completely simulate the measurement of detecting the time shift τ based on the AWVA technique shown in

Fig. 1, the system is pre-selected into a polarized state

$$|\Phi_i\rangle = \sin\left(\frac{\pi}{4}\right)|H\rangle + \cos\left(\frac{\pi}{4}\right)|V\rangle = \frac{1}{\sqrt{2}}(|H\rangle + |V\rangle), \quad (1)$$

where $|H\rangle$ and $|V\rangle$ represent the horizontally and vertically polarized states respectively. Thus, the initial joint state of the system and the pointer is given by

$$|\Phi_i\rangle \otimes |\Psi_i\rangle = \frac{1}{\sqrt{2}}(|H\rangle + |V\rangle)|\Psi_i\rangle, \quad (2)$$

Meanwhile, the initial pointer with the Gaussian profile is prepared by the modulator in the time domain:

$$I_1^{in}(t) = |\langle q|\Psi_i\rangle|^2 = I_0 \frac{1}{(2\pi\zeta^2)^{1/4}} e^{-(t-t_0)^2/4\zeta^2}. \quad (3)$$

where I_0 represents the normalized factor, and ζ represents the pointer spread. Then, the system and the pointer are weakly coupled with the interaction Hamiltonian $\hat{H} = \tau\hat{A} \otimes \hat{p}$, where the observable operator satisfies $\hat{A} = |H\rangle\langle H| - |V\rangle\langle V|$ and \hat{p} is the momentum operator conjugate to the position operator \hat{q} [16, 17, 21, 27]. It is worth noting that the AWVA technique needs two signals from two auto-correlative channels, one of the signals comes from the weak measurement for detecting shift τ and we call it the “measurement channel”. Correspondingly, another signal retains the information of the initial pointer without the weak interaction and did not change with the time shift τ , and we call it “reference channel”. According to the principle of the standard weak measurement, the final state of the pointer in the measurement channel is given by:

$$\begin{aligned} |\Psi_{f1}\rangle &= \langle\Phi_f| e^{-i\tau\hat{A} \otimes \hat{p}} |\Psi_i\rangle |\Phi_i\rangle \\ &\approx \langle\Phi_f| \left[1 - i\tau\hat{A} \otimes \hat{p}\right] |\Psi_i\rangle |\Phi_i\rangle \\ &= \langle\Phi_f|\Phi_i\rangle [1 - i\tau A_w \hat{p}] |\Psi_i\rangle \\ &= \langle\Phi_f|\Phi_i\rangle e^{-i\tau A_w \hat{p}} |\Psi_i\rangle, \end{aligned} \quad (4)$$

where $A_w := \langle\Phi_f|\hat{A}|\Phi_i\rangle/\langle\Phi_f|\Phi_i\rangle$ is the so-called weak value [16], which represents the mean value of observable \hat{A} . Note that the approximation in Eq. (4) only holds in the weak-measurement region, where the time shift τ is much smaller than the pointer spread ζ . Normally, the weak value A_w is a complex number [48], whose real part is associated with the pointer shift in position space, while its imaginary part is associated with the pointer shift in momentum space. In this paper, the weak measurement works in the time domain, the time shift τ in the position of the pointer is amplified by the real part of A_w [49]:

$$\Delta\langle\hat{q}\rangle = \frac{\int dq q |\langle q|\Psi_f\rangle|^2}{\int dq |\langle q|\Psi_f\rangle|^2} = \tau \text{Re}[A_w]. \quad (5)$$

To amplify the ultra-small time shift τ , the system is post-selected into the state:

$$|\Phi_f\rangle = \sin\left(-\frac{\pi}{4} + \alpha\right)|H\rangle + \cos\left(-\frac{\pi}{4} + \alpha\right)|V\rangle, \quad (6)$$

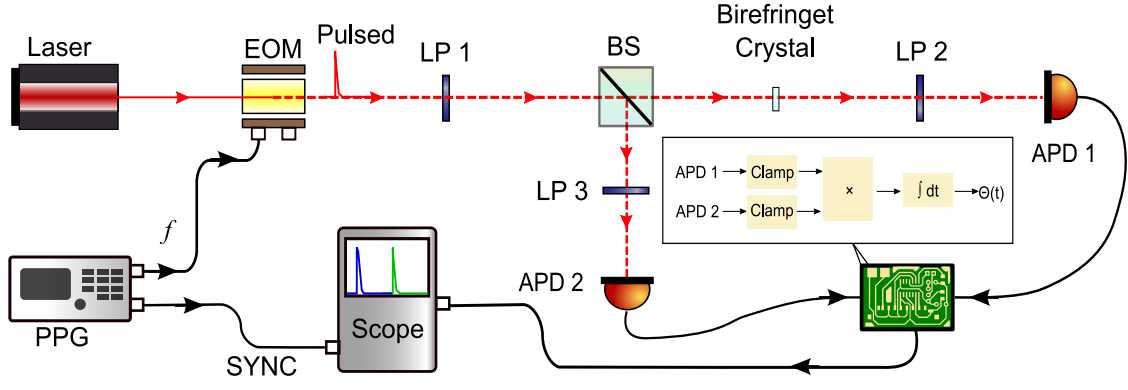


FIG. 1. Scheme of the standard AWVA technique. The Gaussian pulse is produced by the laser and electro-optic modulator (EOM). Where the EOM is controlled by the programmable single pulse generator (PPG). Then photons are pre-selected by the Polarizer 1 (LP1) with an optical axis set at 45° . Then the beam is divided by a 50:50 beam splitter (BS) for an auto-correlative measurement. The horizontal light path corresponds to the standard weak measurement in the time domain. A time delay τ (corresponding to a phase shift between the horizontally polarized state $|H\rangle$ and vertically polarized state $|V\rangle$) is induced by a birefringent crystal. Then, the photons are post-selected by the Polarizer 2 (LP2) with an optical axis set at $\alpha - 45^\circ$, and the arrival time of single photons is measured with an avalanche photodiode (APD1). The vertical path is corresponding to an auto-correlative measurement. The optical axis of polarizer 3 (LP3) is also set at $\alpha - 45^\circ$, and photon arrival times are measured with an avalanche photodiode (APD2). Finally, the detected signals at APD1 and APD1 passed through the voltage-clamp module (Clamp), the product module (\times), and the integral module ($\int dt$). The oscilloscope (Scope) synchronizes time with PPG by SYNC line and displays the measured quantity $\Theta(\tau)$.

where α should not be chosen as $\alpha=0$ to obtain the non-vanishing probability of post-selection. One then obtains the weak value as:

$$A_w = \frac{\sin(-\frac{\pi}{4} + \alpha) - \cos(\frac{\pi}{4} + \alpha)}{\sin(-\frac{\pi}{4} + \alpha) + \cos(\frac{\pi}{4} + \alpha)} = -\cot\alpha, \quad (7)$$

the corresponding time shift τ can be obtained from the peak shift $\delta t = |\tau \text{Re} A_w| = \tau \cot\alpha$ of the signal detected by an avalanche photodiode (APD1), with the detected signal I_1^{out} calculated from Eq. (4) as:

$$\begin{aligned} I_1^{out}(t; \tau) &= |\langle \Phi_f | \Phi_i \rangle|^2 e^{-2i\tau A_w \hat{p}} |\langle q | \Psi_i \rangle|^2 \\ &\approx \frac{I_0}{2} \frac{(\sin\alpha)^2}{(2\pi\zeta^2)^{1/4}} e^{-(t-t_0-\delta t)^2/4\zeta^2}. \end{aligned} \quad (8)$$

For the measurement in the reference channel, the final state $|\Psi_{f2}\rangle$ of the pointer in the measurement channel is given by:

$$\begin{aligned} |\Psi_{f2}\rangle &= \langle \Phi_f | e^{-i\tau \hat{A} \otimes \hat{p}} | \Psi_i \rangle | \Phi_i \rangle |_{\tau=0} \\ &\approx \langle \Phi_f | \left[1 - i\tau \hat{A} \otimes \hat{p} \right] | \Psi_i \rangle | \Phi_i \rangle |_{\tau=0} \\ &= \langle \Phi_f | \Phi_i \rangle [1 - i\tau A_w \hat{p}] | \Psi_i \rangle |_{\tau=0} \\ &= \langle \Phi_f | \Phi_i \rangle e^{-i\tau A_w \hat{p}} | \Psi_i \rangle |_{\tau=0} \\ &= \langle \Phi_f | \Phi_i \rangle | \Psi_i \rangle, \end{aligned} \quad (9)$$

and the signal detected by an avalanche photodiode (APD2) can be calculated by

$$\begin{aligned} I_2^{out}(t; \tau = 0) &= |\langle \Phi_f | \Phi_i \rangle|^2 |\langle q | \Psi_i \rangle|^2 \\ &\approx \frac{I_0}{2} \frac{(\sin\alpha)^2}{(2\pi\zeta^2)^{1/4}} e^{-(t-t_0)^2/4\zeta^2}. \end{aligned} \quad (10)$$

Note that the source of the various noise may have a different impact on the AWVA technique. When only the traditional quantum weak measurement scheme in an open system is considered, weak values have been widely investigated including providing specific expressions of weak values in various noises background [3–5, 50, 51]. However, these works do not show the final signal (corresponding to the pointer in the time domain or in the frequency domain), since the detection noise on APDs and electrical noise will inevitably disturb the signals $I_1^{out}(t; \tau)$ and $I_2^{out}(t; \tau = 0)$ with a negative-dB SNR. Theoretically, it is challenging and difficult to investigate the influence of noises from different sources on the WVA technique and the AWVA technique. In this paper, we simulate the AWVA measurements under non-Gaussian noises with a simple assumption that the effect from all sources of noises is equivalent to adding a certain type of noise on APDs.

In order to discuss the influence of various non-Gaussian noises on the AWVA technique, the noises are assumed to be added directly to the final measured signal $I_1^{out}(t; \tau)$ at APD1 and $I_2^{out}(t; \tau)$ at APD2. Then we obtain the quantity Θ in the AWVA scheme with the noises $\mathbf{N}(t, \xi_1)$ and $\mathbf{N}(t, \xi_2)$, where ξ_1 and ξ_2 represent the initial times of the noises. According to the auto-correlation technique for signal denoising in engineering [52–54], the

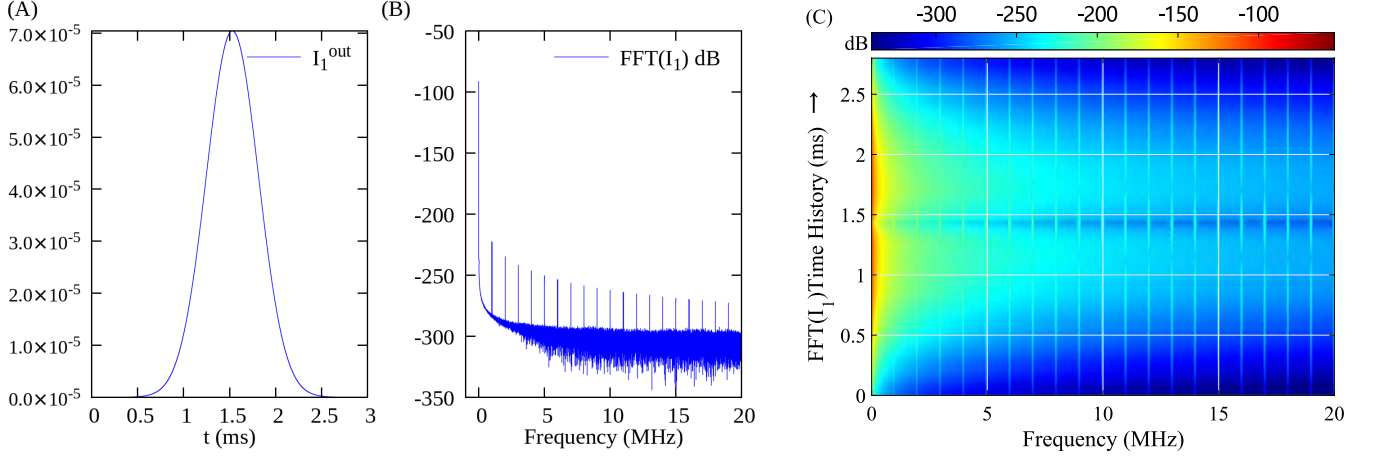


FIG. 2. Time domain and frequency domain characteristics of signals: (A) the final pointer in the time domain, (B) the FFT results, and (C) the time history of the FFT result.

$\Theta(\tau)$ is defined as

$$\begin{aligned}
 & \Theta(\tau) \\
 &= \int_0^t [I_1^{out}(t'; \tau) + \mathbf{N}(t', \xi_1)] \times [I_2^{out}(t') + \mathbf{N}(t', \xi_2)] dt' \\
 &= \int_0^t I_1^{out}(t'; \tau) \times I_2^{out}(t') dt' + \int_0^t I_1^{out}(t'; \tau) \times \mathbf{N}(t', \xi_2) dt' \\
 &+ \int_0^t \mathbf{N}(t', \xi_1) \times I_1^{out}(t'; \tau) dt' + \int_0^t \mathbf{N}(t', \xi_1) \times \mathbf{N}(t', \xi_2) dt'.
 \end{aligned} \tag{11}$$

We can define

$$\Theta_{II}(\tau) = \int_0^t I_1^{out}(t'; \tau) \times I_2^{out}(t') dt', \tag{12}$$

$$\Theta_{IN}(\tau) = \int_0^t I_1^{out}(t'; \tau) \times \mathbf{N}(t', \xi_2) dt', \tag{13}$$

$$\Theta_{NI}(\tau) = \int_0^t \mathbf{N}(t', \xi_1) \times I_1^{out}(t'; \tau) dt', \tag{14}$$

$$\Theta_{NN}(\tau) = \int_0^t \mathbf{N}(t', \xi_1) \times \mathbf{N}(t', \xi_2) dt', \tag{15}$$

where $\Theta_{II}(\tau)$ represents the desirable results of the AWVA scheme without the noise, $\Theta_{IN}(\tau)$ and $\Theta_{NI}(\tau)$ represent the non-correlation between the signal and the random noise, $\Theta_{NN}(\tau)$ represents the non-correlation between different noises. Note that our previous work [43] shows that the AWVA scheme has good robustness under the present of Gaussian noise when sufficiently long times lead to the relationship $\Theta(\tau) = \Theta_{II}(\tau)$. In this paper, $\Theta(\tau)$ can be obtained by simulating the signal processing module shown in the circuit of Fig. 1 on Simulink. It is worth noting that there is an additional electrical “voltage-clamp” module ¹ in Fig. 1 compared with our

previous work [43]. This signal processing module is designed for inducing the effect of peak noise—the frequency-nonstationary colored noise, and we will show and discuss the details in the next section.

B. The non-Gaussian noises

It has been pointed out that noise [41, 55, 56] has a great influence on the weak measurement. To simulate the AWVA schemes in a realistic situation, the effects of various types of noise are studied, including optical noise from the instability of the light source, interference in the light path, thermal noise, and shot noise of the detection, and noise from other unknown sources. Numerous studies [2, 57, 58] on the noise-induced phenomena indicated that the noises in most fields of physics obey the Gaussian distribution, and our previous work assumed that all noises can be approximately simplified as having a Gaussian normal distribution [43] denoted as $\mathbf{N}_0(t, \sigma^2)$, where σ^2 is the variance of the random signal. However, recent works [1–5] with more realistic physical models investigate more on non-Gaussian (colored) noises. In addition, there is experimental evidence pointing to the fact that, for gravitational wave observations [9–12], the noise sources could be non-Gaussian. Note that the basic detection scheme for gravitational waves involves measuring the phase or intensity in the interference of laser light, similar to our weak measure schemes. Therefore, we study the AWVA schemes in the presence of the frequency-stationary and frequency-nonstationary colored noises. The characterization of the frequency-stationary colored noise is that the spectrum does not change with time, while the spectrum of the frequency-nonstationary colored noise varies over time.

Normally, colored noises can be generated using the Box-Mueller algorithm [44]. However, we adopt an alternative technique for generating the frequency-stationary colored noises by choosing specific regions of frequency

¹ The “voltage-clamp” module of the control system prevents the voltage from rising above a certain threshold value.

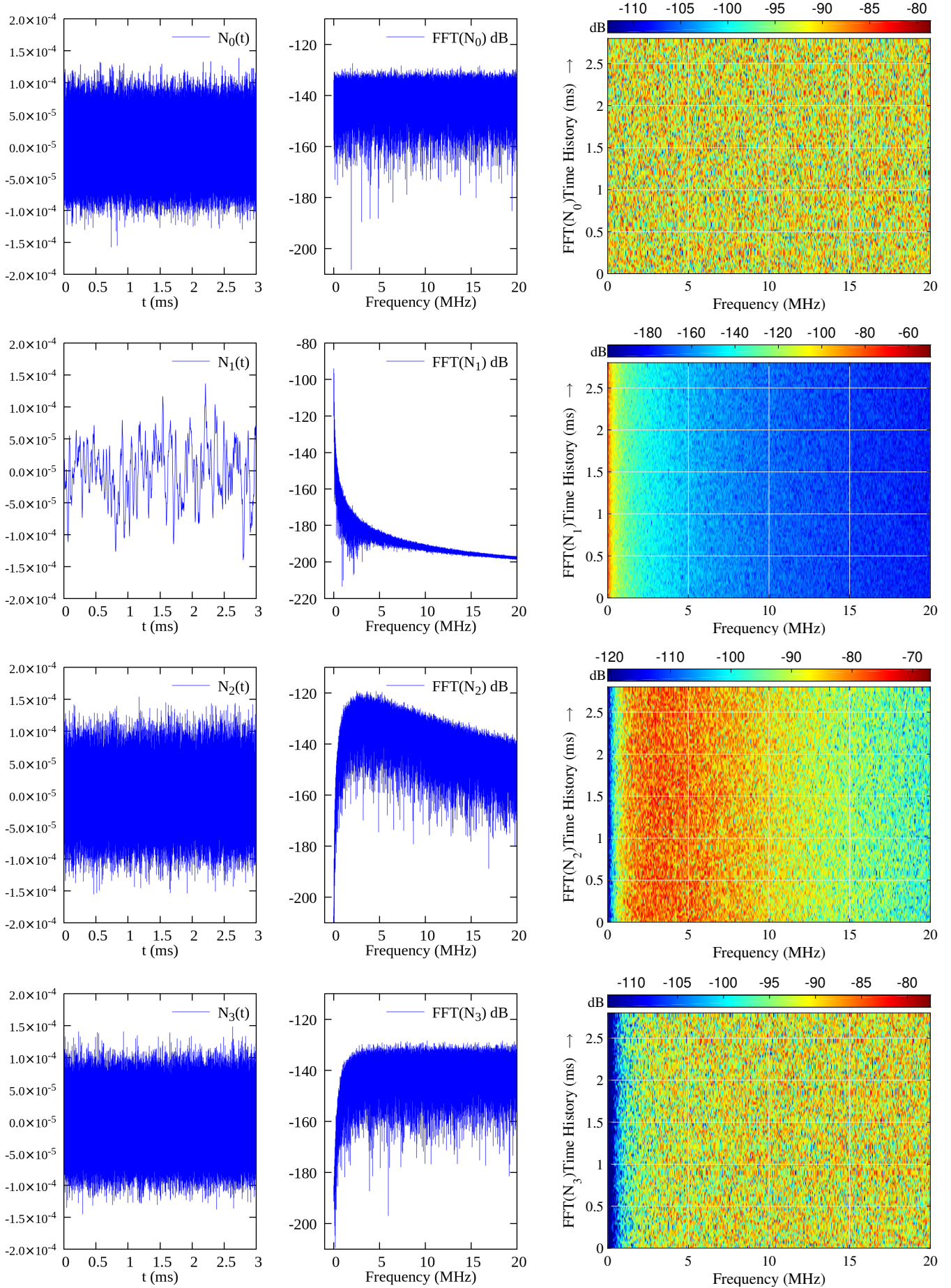


FIG. 3. The various frequency-stationary noises in the time domain (left panels), the FFT results (middle panels) and the time history of the FFT results (right panels).

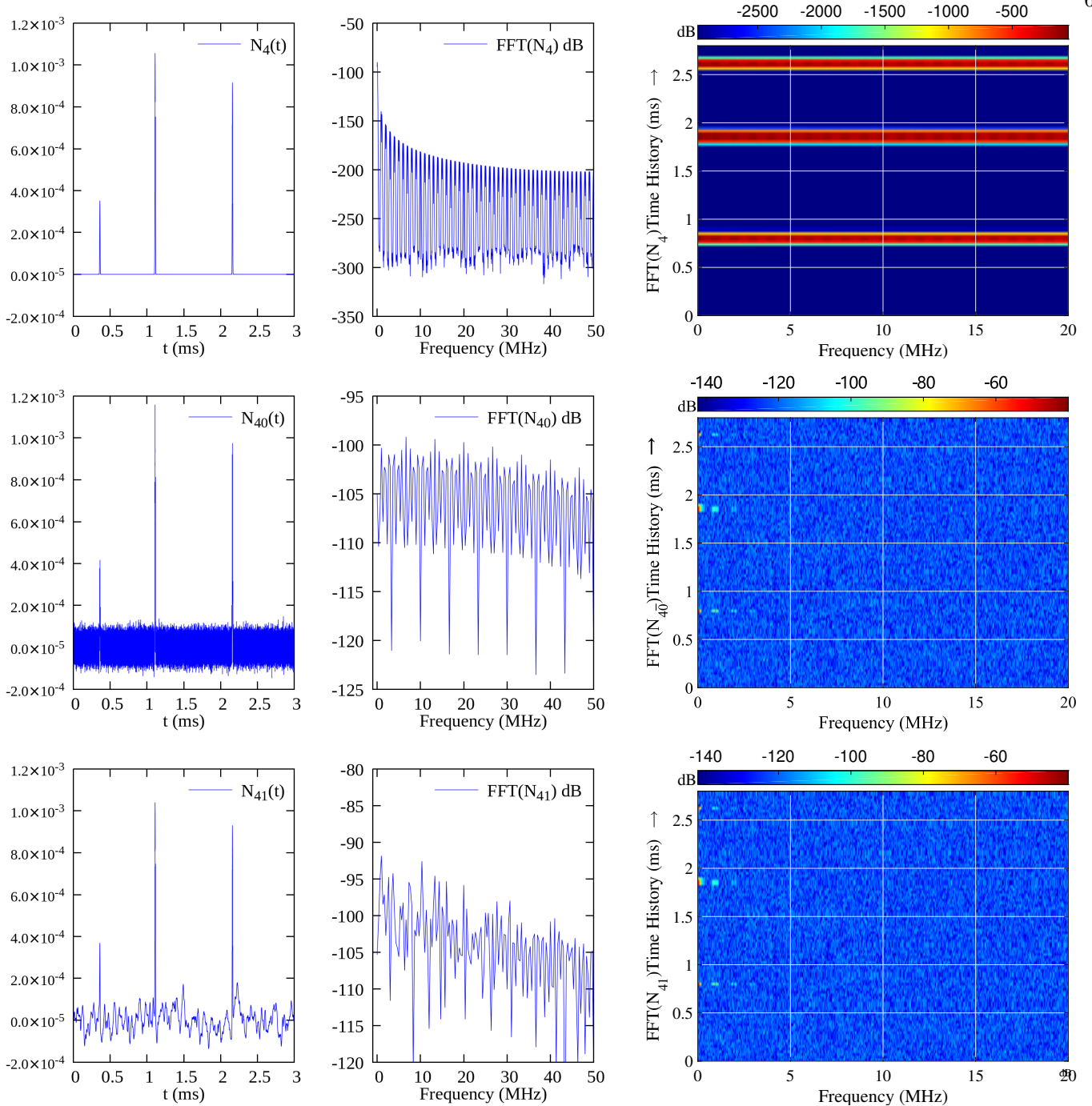


FIG. 4. The various frequency-nonstationary noises in the time domain (left panels), the FFT results (middle panels) and the time history of the FFT results (right panels). Noise “ N_{40} ” represents the combination of the impulsive noise N_4 and the Gaussian noise N_0 . Noise “ N_{41} ” represents the combination of the impulsive noise N_4 and the $1/f$ noise N_1 . Noise “ N_{40} ” represents the combination of the impulsive noise N_4 and 0.1 times Gaussian noise N_0 . Note that the time history of N_{40} can not distinctly display the character of frequency-nonstationary noise.

spectrum of the Gaussian white noise $\mathbf{N}_0(t, \sigma^2)$. Specifically, we generate three types of frequency-stationary colored noise $\mathbf{N}_1(t, \sigma^2)$, $\mathbf{N}_2(t, \sigma^2)$ and $\mathbf{N}_3(t, \sigma^2)$:

$$\mathcal{L}[\mathbf{N}_1(t, \sigma^2)] = \mathcal{G}_1(s) \times \mathcal{L}[\mathbf{N}_0(t, \sigma^2)], \quad (16)$$

$$\mathcal{L}[\mathbf{N}_2(t, \sigma^2)] = \mathcal{G}_2(s) \times \mathcal{L}[\mathbf{N}_0(t, \sigma^2)], \quad (17)$$

$$\mathcal{L}[\mathbf{N}_3(t, \sigma^3)] = \mathcal{G}_3(s) \times \mathcal{L}[\mathbf{N}_0(t, \sigma^3)], \quad (18)$$

where the function \mathcal{L} represents the Laplace transformation $\mathcal{L}[\mathbf{N}_0(t, \sigma^2)] = \int_0^\infty \mathbf{N}_0(t, \sigma^2) e^{-st} dt$. $\mathcal{G}_1(s)$, $\mathcal{G}_2(s)$ and $\mathcal{G}_3(s)$ correspond to the transfer functions for generating noises with low frequency, medium frequency and high frequency respectively:

$$\mathcal{G}_1(s) = \mathcal{G}_{11}(s) \times \mathcal{G}_{11}(s), \quad (19)$$

$$\mathcal{G}_2(s) = \mathcal{G}_{21}(s) \times \mathcal{G}_{21}(s) \times \mathcal{G}_{22}(s) \times \mathcal{G}_{23}(s), \quad (20)$$

$$\mathcal{G}_3(s) = \mathcal{G}_{31}(s) \times \mathcal{G}_{31}(s). \quad (21)$$

where $\mathcal{G}_{11}(s) = 1000/(s + 100)$, $\mathcal{G}_{22}(s) = 10000/(s + 10000)$ and $\mathcal{G}_{23}(s) = 83000/(s + 10000)$ represent the first order low-pass filters. $\mathcal{G}_{21}(s) = s/(s + 40000)$ and $\mathcal{G}_{31}(s) = s/(s + 8000)$ represents the first order high-pass filters.

In this paper, we use three Gaussian pulses with different intensity and width to generate frequency-nonstationary colored noise $\mathbf{N}_4(t, \sigma^2)$:

$$\begin{aligned} \mathbf{N}_4(t) = & \frac{\Gamma_{41}}{(2\pi\zeta_4^2)^{1/4}} e^{-\frac{(t-t_{01})^2}{\kappa_{41}\zeta_4^2}} + \frac{\Gamma_{42}}{(2\pi\zeta_4^2)^{1/4}} e^{-\frac{(t-t_{02})^2}{\kappa_{42}\zeta_4^2}} \\ & + \frac{\Gamma_{43}}{(2\pi\zeta_4^2)^{1/4}} e^{-\frac{(t-t_{03})^2}{\kappa_{43}\zeta_4^2}} \end{aligned} \quad (22)$$

where $\zeta_4^2 = 0.0002^2$ represents the spread of the Gaussian pulses. Other parameters are used to change the profile of the Gaussian pulses and are set randomly: $\Gamma_{41} = 15$, $\Gamma_{42} = 5$, $\Gamma_{43} = 9$, $t_{01} = 0.00255$ s, $t_{02} = 0.0018$ s, $t_{03} = -0.00015$ s, $\kappa_{41} = 0.0016$, $\kappa_{42} = 0.0016$, $\kappa_{43} = 0.0012$.

Realistically various kinds of noise are expected to contribute to the detected signals. Therefore, we add the frequency-nonstationary colored noise $\mathbf{N}_4(t, \zeta^2)$ into the frequency-stationary colored noise:

$$\mathbf{N}_{40}(t) = \mathbf{N}_4(t, \zeta^2) + \mathbf{N}_0(t, \sigma^2), \quad (23)$$

$$\mathbf{N}_{41}(t) = \mathbf{N}_4(t, \zeta^2) + \mathbf{N}_1(t, \sigma^2). \quad (24)$$

First, we display the spectrum (corresponding to the Fourier transform) and the history of the signal spectrum without noises in Fig. 2. The results show that the energy of the signal is mostly concentrated at low frequencies ($f < 1$ MHz). It is worth noting that the history of the signal spectrum is not stationary when the finite integration time for the FFT transformation is far smaller than the spread of the signal.

Then, the spectrum and its history for the various kinds of colored noise are shown in Figs. 3 and 4:

1). The Gaussian noise $\mathbf{N}_0(t, \sigma^2)$ is also called white noise, because the Fourier transform $\text{FFT}(\mathbf{N}_0)$ is flat. The influence of Gaussian noise on the AWVA technique has been investigated in our previous work [43] and the results show that the AWVA technique outperforms the WVA technique with stronger robustness.

2). The low-frequency noise $\mathbf{N}_1(t, \sigma^2)$ is also called flicker noise or $1/f$ noise, because the Fourier transform FFT_1 shown in Fig. 5 indicates that the noise is proportional to $1/f^\gamma$ (γ is a constant). The $1/f$ noise has captured the attention of researchers from many fields of electronics and physics, and several models with various origins have been proposed to interpret the observed $1/f$ noises in different electronic devices or physical systems. [59].

3). The medium frequency noise $\mathbf{N}_2(t, \sigma^2)$ is studied as a proxy for other noise sources, such as power ripple and electromagnetic interference.

4). The high-frequency noise $\mathbf{N}_3(t, \sigma^2)$ is studied as a contrast to the low-frequency noise $\mathbf{N}_1(t, \sigma^2)$.

5). The frequency-nonstationary colored noises $\mathbf{N}_4(t, \sigma^2)$, $\mathbf{N}_{40}(t, \sigma^2)$ and $\mathbf{N}_{41}(t, \sigma^2)$ are shown in Fig. 4. The time history of FFT results indicate that the spectrum varies over time due to the "peak" (in the time domain) accruing. This kind of noise, called "peak noise" normally arises from the instantaneous surge current caused by electromagnetic interference.

While noise in realistic scenarios may be more complicated than all the above-considered types of noises, it is necessary to consider the effects of these noises on the weak measurements, and the simulation results are shown in the next section.

III. NUMERICAL RESULTS

In this paper, we simulate the AWVA technique for detecting the time delays with the tools in Simulink. There are two reasons to simulate on Simulink, one is that it is convenient to generate various types of colored noise by translating the Gaussian white noise with different band-pass filters, and the other is that Simulink allows us to implement the signal processing module shown in Fig. 1.

In our simulation, the initial temporal probe was chosen as:

$$I_1^{in}(t; \tau) = |\langle q | \Psi_i \rangle|^2 = \frac{I_0}{(2\pi\zeta^2)^{1/4}} e^{-\frac{(t-t_0)^2}{4\zeta^2}}, \quad (25)$$

where I_0 is set as unit, $\zeta^2 = 0.0002^2$ represents the spread of the initial temporal probe, $t_0 = 0.0015$ represents the center of the probe. The angle for post-selection is set at $\alpha = 0.01$ rad. In total, four types of the noises $\mathbf{N}_0(t, \sigma^2)$, $\mathbf{N}_1(t, \sigma^2)$, $\mathbf{N}_2(t, \sigma^2)$ and $\mathbf{N}_3(t, \sigma^2)$ with different seed ξ at a negative-dB SNR are investigated. Following our previous work [43], the SNR detected at APD1 and APD2 is defined as

$$\text{SNR} = 20 \times \log \frac{\text{Max}[I_1^{\text{out}}(t)]}{\text{Max}[\mathbf{N}(t)]}, \quad (26)$$

In this paper, noise is assumed to occur anywhere in the optical path. In order to improve the accuracy of measurement, statistical averaging after multiple N times measurements is used to reduce uncertainty due to experimental errors induced by noises. The mean value $\bar{\Theta}_0$ ($\bar{\Theta}_\tau$) and its standard error $\pm E_0$ (E_τ) of the N measurements with the different time shift τ are obtained by:

$$\bar{\Theta}_0 = \sum_{i=1}^N \Theta_0(i)/N, \quad E_0 = \sqrt{\frac{[\bar{\Theta}_0 - \Theta_0(i)]^2}{N}}, \quad (27)$$

$$\bar{\Theta}_\tau = \sum_{i=1}^N \Theta_\tau(i)/N, \quad E_\tau = \sqrt{\frac{[\bar{\Theta}_\tau - \Theta_\tau(i)]^2}{N}}, \quad (28)$$

where the (i) represents the result of the i th measurement with the different value of ξ , the subscript "0" represents

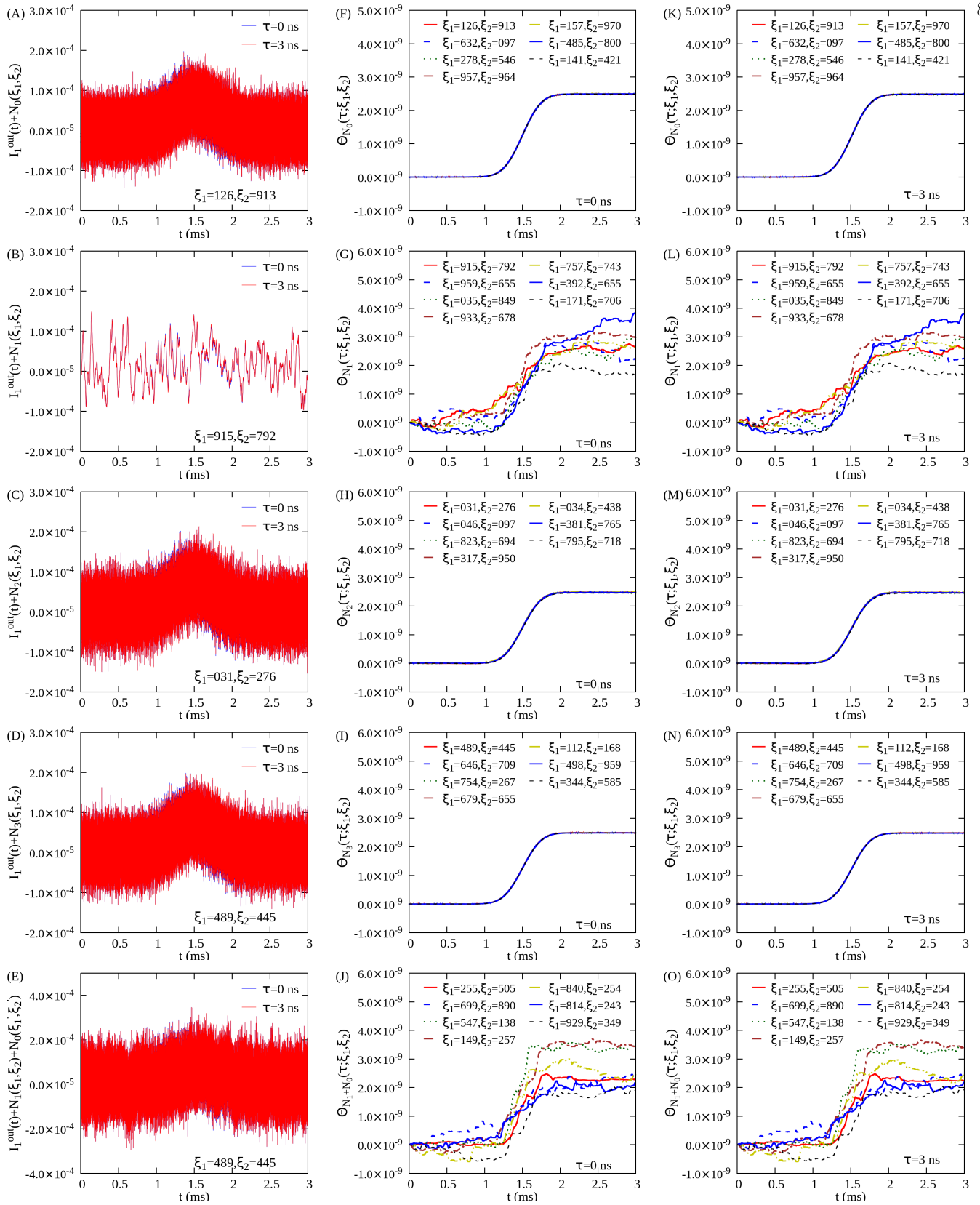


FIG. 5. The simulation results under various frequency-stationary noises. Left panels: the simulation results of detected signals I_1^{out} under noises. Right panels: auto-correlative intensity $\Theta(\tau = 0 \text{ ns})$. Left panels: auto-correlative intensity $\Theta(\tau = 3 \text{ ns})$. Subfigures (A), (F) and (K) represent the results under Gaussian noise N_0 . Subfigures (B), (G) and (L) represent the results under low-frequency noise N_1 . Subfigures (C), (H) and (M) represent the results under medium frequency noise N_1 . Subfigures (D), (I) and (N) represent the results under high-frequency noise N_1 . Subfigures (E), (J) and (O) represent the results under the mixed noise N_1 and N_0 . The seed ξ'_1 and ξ'_2 of noise $N_0(t, \xi)$ in subfigures. (E), (J) and (O) are set as $\xi'_1 = 223$ and $\xi'_2 = 751$.

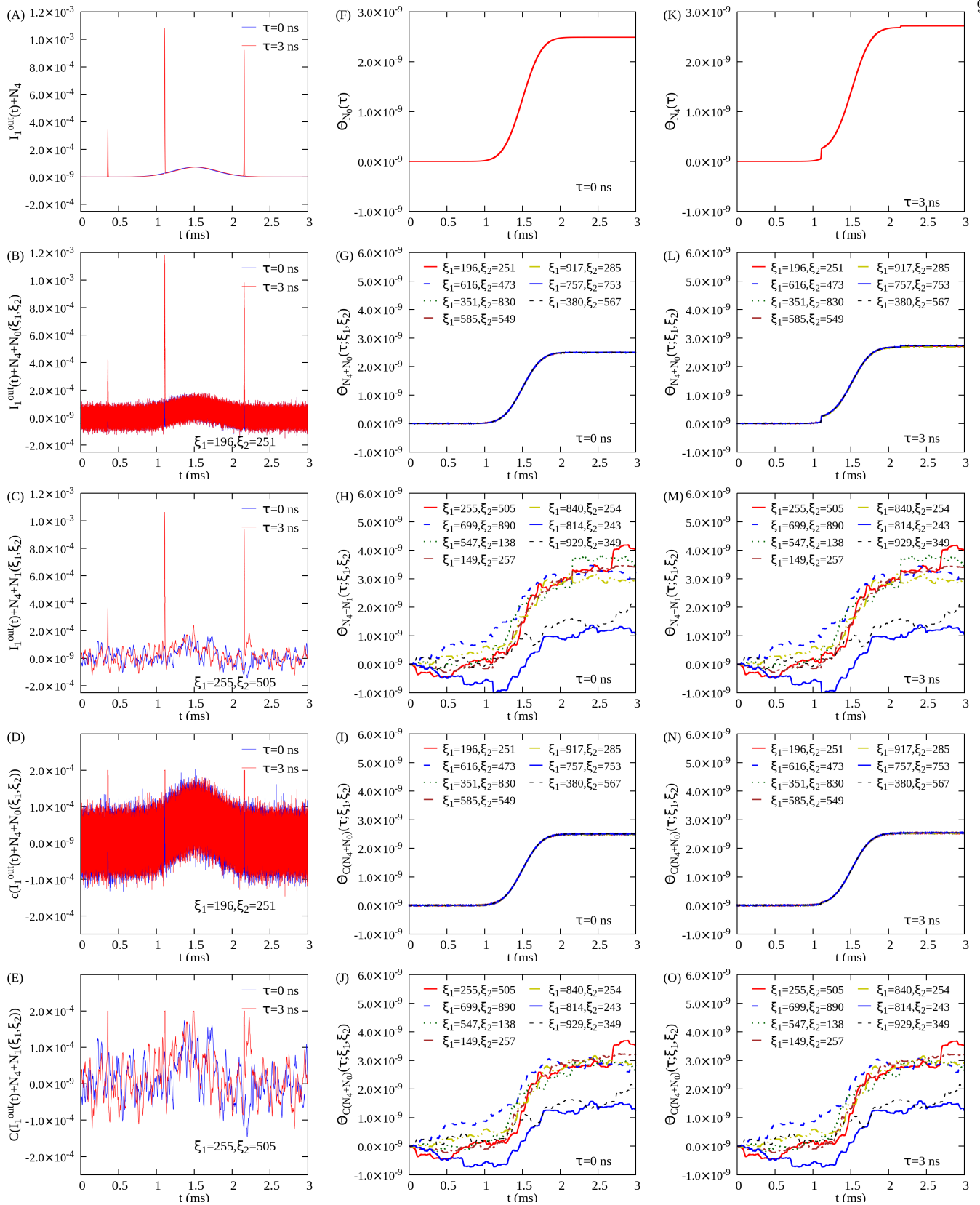


FIG. 6. The simulation results under various frequency-nonstationary noises. Left panels: the simulation results of detected signals I_1^{out} under noises. Right panels: auto-correlative intensity $\Theta(\tau = 0$ ns). Left panels: auto-correlative intensity $\Theta(\tau = 3$ ns). Subfigures (A), (F) and (K) represent the results under peak noise N_4 . Subfigures (B), (G) and (L) represent the results under the mixed noise of N_4 and N_0 . Subfigures (C), (H) and (M) represent the results under the mixed noise of N_4 and N_1 . Subfigures (D), (I) and (N) represent the results under the mixed noise of N_4 and N_0 with voltage-clamp limit. Subfigures (E), (J) and (O) represent the results under the mixed noise of N_4 and N_1 with voltage-clamp limit.

the results of the measurement time shift $\tau = 0$. Finally, the sensitivity $K(t)$ with statistic error $\pm E$ in the AWVA scheme with N measurements is defined as:

$$K(t) = \frac{\Delta[\Theta(t; \tau)]}{\Delta(\tau)} = \frac{\overline{\Theta}_0 - \overline{\Theta}_\tau}{\tau}, \quad E = \frac{E_0 + E_\tau}{2} \quad (29)$$

Note that the sensitivity $K(t)$ depends on the time integral t . The dependence of the sensitivity on t with various types of noise has been discussed in our previous work [43], and one can find that the maximum sensitivity K^M is achieved when integrating to $t = 1.5$ ms. At the same time, the precision of the AWVA technique is strongly dependent on the sampling frequency. Thus, in this paper, we take the sampling frequency $1/T = 100\text{MHz}$ for the numerical simulation on Simulink. The measurements under various noises with different random seed ξ (corresponding different initial times) are shown in Table. II and Table. V. Separately, Table. II displays the results of seven measurements with different ξ of the four *types* of the frequency-stationary noises: the Gaussian noise $\mathbf{N}_0(t, \xi)$, the low-frequency noise $\mathbf{N}_1(t, \xi)$, the medium-frequency noise $\mathbf{N}_2(t, \xi)$, the high-frequency noise $\mathbf{N}_3(t, \xi)$ and the combination of the low-frequency noise $\mathbf{N}_1(t, \xi)$ and the Gaussian noise $\mathbf{N}_0(t, \xi)$. In addition, the results of twenty-one measurements with noise $\mathbf{N}_1(t, \xi)$ and the mixed noise $\mathbf{N}_1(t, \xi) + 3\mathbf{N}_0(t, \xi)$ are shown in Table. III. Table. V displays the seven results with different ξ of the various frequency-nonstationary noises: peak noise $\mathbf{N}_4(t)$, the mixed noise $\mathbf{N}_4(t) + \mathbf{N}_0(t, \xi)$, the mixed noise $\mathbf{N}_4(t) + \mathbf{N}_1(t, \xi)$, voltage-clamp limiting noise $C(\mathbf{N}_4(t) + \mathbf{N}_0(t, \xi))$ and voltage-clamp limiting noise $C(\mathbf{N}_4(t) + \mathbf{N}_1(t, \xi))$.

Finally, some typical results of the signal $I_1^{\text{out}(t)}$, Θ_0 and Θ_τ with different frequency-stationary noise are shown in Fig. 5. While these results with different frequency-nonstationary noises are shown in Fig. 6. After obtaining the results of multiple measurements shown in Tables II, III and V, the final results including the statistical errors along with various noises were determined as shown in Table. I and Fig. 7. On this basis, we compare the sensitivity and the stability of the AWVA scheme with different noises and some possible approaches to enhance the robustness.

A. Effects of frequency-stationary noises

Fig. 3 shows the simulation results of the final measurement signals $I_1^{\text{out}(t)}$, the auto-correlative intensity $\Theta(\tau = 0\text{ns})$ and the auto-correlative intensity $\Theta(\tau = 3\text{ns})$ under various frequency-stationary noises. At the same level (SNR) of noise, the low-frequency noise $\mathbf{N}_1(t, \sigma^2)$ has greater impact on the estimation of $\Theta(\tau)$. A more quantitative and intuitive description—the normalized sensitivity—is displayed in Fig. 7(A). Both the mean value deviation (corresponding to the absolute value of $1 - K/0.0258$) and the error bar under the low-frequency

noise $\mathbf{N}_1(t, \sigma^2)$ are larger than that under other noises. We can trace this poor performance of the AWVA technique under low-frequency noises back to the definition of autocorrelation intensity Θ . According to our previous study [43] on the effect of the sampling frequency (corresponding to the number of sampling points in the period of time 3ms), increasing the sampling frequency can enhance the precision under the Gaussian noise. However, the AWVA technique performs badly when measurements are disturbed by low-frequency noises even at high sample frequency. The main reason is that the low-frequency noise $\mathbf{N}_1(t, \sigma^2)$ as shown in Fig. 3 does not exhibit randomness in the finite time (3ms), and this non-random behavior (meaning $\Theta_{\text{NN}} \gg 0$) can hardly satisfy the relationship $\Theta(\tau) \approx \Theta_{\text{II}}(\tau)$.

In the principle of the signal processing [60], the low-frequency ($1/f$) noises can be reduced by designing the adaptive filters. Nevertheless, the filtering denoising technique does not work under the low-frequency noise since the measurement signal is also low frequency as shown in Fig. 2. Based on the fact that the spectrum of the low-frequency noise $\mathbf{N}_1(t, \sigma^2)$ and the measurement signal are overlapping in the low-frequency domain, we propose a possible solution by increasing the frequency of the Gaussian signal at the cost of decreasing the intensity of $\Theta(\tau)$ and the sensitivity of the AWVA scheme. This is because increasing the frequency of the Gaussian signal will cut down the pointer spread ζ and lead to a smaller integral time t for estimating $\Theta(\tau)$. In addition, the low-frequency noise ($1/f$) has been widely studied and can be reduced by lowering the temperature of the device [59].

In this work, we propose another possible solution to reducing the adverse impact of the low-frequency noise $\mathbf{N}_1(t, \sigma^2)$ by adding additive Gaussian noise with a given intensity. In Table I, Fig. 7(B) and Fig. 7(C), we display the results of the combination of the low-frequency noise $\mathbf{N}_1(t, \sigma^2)$ and the Gaussian noise $\mathbf{N}_0(t, \sigma^2)$. The results of 7 measurements in Fig. 7(B) indicate that the measurement under noises $\mathbf{N}_1 + 2\mathbf{N}_0$ and $\mathbf{N}_1 + 3\mathbf{N}_0$ have smaller deviations of the theoretical value but with larger error bars. In addition, the measurement under noises $\mathbf{N}_1 + \mathbf{N}_0$ performs worse than the measurement under noises \mathbf{N}_1 . Note that this unusual result may be due to the number of measurements. If we change the seed of $\mathbf{N}_1(t, \sigma^2)$, other different qualitative results may be obtained. The reason is the non-random behavior in finite 3 ms time of the low-frequency noise $\mathbf{N}_1(t, \sigma^2)$, even when seven measurements are conducted. Theoretically, increasing the number of measurements can better reflect the randomness of noise and avoid accidental results.

Then, the simulation results with 21 measurements are investigated and the normalized sensitivity are shown in Table I and Fig. 7(C). The details of the simulation under noises \mathbf{N}_1 , $\mathbf{N}_1 + 1\mathbf{N}_0$, $\mathbf{N}_1 + 2\mathbf{N}_0$ and $\mathbf{N}_1 + 3\mathbf{N}_0$ can be found in Table III, we market the noises $(\mathbf{N}_1)^*$, $(\mathbf{N}_1 + 1\mathbf{N}_0)^*$ and $(\mathbf{N}_1 + 3\mathbf{N}_0)^*$ as the results with 21 measurements and calculate the corresponding deviation of the theoretical value with error bars. Fig. 7(C) in-

TABLE I. Parameters and some characteristic numerical results of measuring time shift $\tau = 0.0$ ns and time shift $\tau = 3.0$ ns under various noises in the AWVA scheme. The contents in parentheses represent statistical errors. The expression (...) * represents the results with 21 measurements. The expression (...) ** represents the results with 87 measurements. The expression (...) + represents the results with the chosen measurement range of $1.0 \times 10^{-9} < \Theta < 1.6 \times 10^{-9}$. The expression C(...) represents the results with the voltage-clamp approach.

Noise	SNR dB		$\bar{\Theta}_0$	$\bar{\Theta}_\tau$	$K = \Delta \bar{\Theta}_\tau / \tau$	$K/0.0258$
no noise			1.2442×10^{-9}	1.1666×10^{-9}	0.0258	1.000(± 0.000)
\mathbf{N}_0	-5.1	$1.2459 \times 10^{-9} (\pm 0.0048 \times 10^{-9})$	$1.1682 \times 10^{-9} (\pm 0.0047 \times 10^{-9})$	$0.0259 (\pm 0.0031)$	1.004(± 0.122)	
\mathbf{N}_1	-5.1	$1.3066 \times 10^{-9} (\pm 0.3047 \times 10^{-9})$	$1.2208 \times 10^{-9} (\pm 0.3144 \times 10^{-9})$	$0.0286 (\pm 0.2063)$	1.108(± 7.998)	
\mathbf{N}_2	-5.1	$1.2399 \times 10^{-9} (\pm 0.0153 \times 10^{-9})$	$1.1622 \times 10^{-9} (\pm 0.0153 \times 10^{-9})$	$0.0259 (\pm 0.0102)$	1.004(± 0.395)	
\mathbf{N}_3	-5.1	$1.2456 \times 10^{-9} (\pm 0.0034 \times 10^{-9})$	$1.1677 \times 10^{-9} (\pm 0.0035 \times 10^{-9})$	$0.0259 (\pm 0.0023)$	1.006(± 0.089)	
$\mathbf{N}_1 + 1\mathbf{N}_0$	-11.0	$1.5114 \times 10^{-9} (\pm 0.5998 \times 10^{-9})$	$1.4091 \times 10^{-9} (\pm 0.5516 \times 10^{-9})$	$0.0341 (\pm 0.3838)$	1.321(± 14.87)	
$\mathbf{N}_1 + 2\mathbf{N}_0$	-14.5	$1.4664 \times 10^{-9} (\pm 0.5742 \times 10^{-9})$	$1.3825 \times 10^{-9} (\pm 0.5488 \times 10^{-9})$	$0.0279 (\pm 0.3743)$	1.089(± 14.51)	
$\mathbf{N}_1 + 3\mathbf{N}_0$	-17.0	$1.4283 \times 10^{-9} (\pm 0.4818 \times 10^{-9})$	$1.3448 \times 10^{-9} (\pm 0.4645 \times 10^{-9})$	$0.0278 (\pm 0.3154)$	1.078(± 12.22)	
$(\mathbf{N}_1)^*$	-5.1	$1.4087 \times 10^{-9} (\pm 0.5695 \times 10^{-9})$	$1.3227 \times 10^{-9} (\pm 0.5621 \times 10^{-9})$	$0.0286 (\pm 0.3772)$	1.108(± 14.62)	
$(\mathbf{N}_1 + 1\mathbf{N}_0)^*$	-11.0	$1.1465 \times 10^{-9} (\pm 0.5157 \times 10^{-9})$	$1.0631 \times 10^{-9} (\pm 0.4931 \times 10^{-9})$	$0.0278 (\pm 0.3362)$	1.077(± 13.03)	
$(\mathbf{N}_1 + 2\mathbf{N}_0)^*$	-14.5	$1.1124 \times 10^{-9} (\pm 0.5041 \times 10^{-9})$	$1.0354 \times 10^{-9} (\pm 0.4924 \times 10^{-9})$	$0.0256 (\pm 0.3321)$	0.994(± 12.87)	
$(\mathbf{N}_1 + 3\mathbf{N}_0)^*$	-17.0	$1.0717 \times 10^{-9} (\pm 0.5056 \times 10^{-9})$	$0.9966 \times 10^{-9} (\pm 0.4919 \times 10^{-9})$	$0.0248 (\pm 0.3325)$	0.963(± 12.88)	
$(\mathbf{N}_1 + 3\mathbf{N}_0)^{**}$	-17.0	$1.2247 \times 10^{-9} (\pm 0.5173 \times 10^{-9})$	$1.1479 \times 10^{-9} (\pm 0.5179 \times 10^{-9})$	$0.0256 (\pm 0.3450)$	0.992(± 13.37)	
$(\mathbf{N}_1 + 3\mathbf{N}_0)^+$	-17.0	$1.3537 \times 10^{-9} (\pm 0.1846 \times 10^{-9})$	$1.2718 \times 10^{-9} (\pm 0.1830 \times 10^{-9})$	$0.0273 (\pm 0.1225)$	1.054(± 4.749)	
\mathbf{N}_4	-23.5	$1.2443 \times 10^{-9} (\pm 0.0000 \times 10^{-9})$	$1.3707 \times 10^{-9} (\pm 0.0000 \times 10^{-9})$	$-0.0421 (\pm 0.0000)$	$-1.633 (\pm 0.000)$	
$\mathbf{N}_4 + \mathbf{N}_0$	-23.7	$1.2473 \times 10^{-9} (\pm 0.0054 \times 10^{-9})$	$1.3683 \times 10^{-9} (\pm 0.0131 \times 10^{-9})$	$-0.0403 (\pm 0.0061)$	$-1.563 (\pm 0.233)$	
$\mathbf{N}_4 + \mathbf{N}_1$	-23.7	$1.4008 \times 10^{-9} (\pm 0.8167 \times 10^{-9})$	$1.3347 \times 10^{-9} (\pm 0.8104 \times 10^{-9})$	$0.0220 (\pm 0.5423)$	0.854(± 21.02)	
C($\mathbf{N}_4 + \mathbf{N}_0$)	-9.1	$1.2473 \times 10^{-9} (\pm 0.0054 \times 10^{-9})$	$1.2085 \times 10^{-9} (\pm 0.0058 \times 10^{-9})$	$0.0129 (\pm 0.0037)$	0.501(± 0.144)	
C($\mathbf{N}_4 + \mathbf{N}_0$) *	-9.1	$1.2443 \times 10^{-9} (\pm 0.0057 \times 10^{-9})$	$1.2061 \times 10^{-9} (\pm 0.0059 \times 10^{-9})$	$0.0127 (\pm 0.0038)$	0.493(± 0.149)	
C($\mathbf{N}_4 + \mathbf{N}_1$)	-9.1	$1.3242 \times 10^{-9} (\pm 0.6598 \times 10^{-9})$	$1.2586 \times 10^{-9} (\pm 0.6545 \times 10^{-9})$	$0.0218 (\pm 0.4381)$	0.847(± 16.98)	
C($\mathbf{N}_4 + \mathbf{N}_1$) **	-9.1	$1.4561 \times 10^{-9} (\pm 0.7051 \times 10^{-9})$	$1.3764 \times 10^{-9} (\pm 0.7052 \times 10^{-9})$	$0.0265 (\pm 0.4701)$	1.029(± 18.22)	
C($\mathbf{N}_4 + \mathbf{N}_1$) +	-9.1	$1.2429 \times 10^{-9} (\pm 0.1534 \times 10^{-9})$	$1.1620 \times 10^{-9} (\pm 0.1566 \times 10^{-9})$	$0.0269 (\pm 0.1033)$	1.045(± 4.005)	

indicates that adding the Gaussian noise $\mathbf{N}_0(t, \sigma^2)$ to the measurements under the low-frequency noise $\mathbf{N}_1(t, \sigma^2)$ can result in more precise results with smaller deviations of the theoretical value and error bars. In particular, it is shown that adding twice the intensity of the Gaussian noise $\mathbf{N}_0(t, \sigma^2)$ into the low-frequency noise $\mathbf{N}_1(t, \sigma^2)$ has the smallest deviations than adding other levels of noise $\mathbf{N}_0(t, \sigma^2)$. It is worth noting that the conclusion is only valid for this specific low-frequency noise $\mathbf{N}_1(t, \sigma^2)$ in this paper. Further experiments on the AWVA measurements under other types of low-frequency noise $\mathbf{N}_1(t, \sigma^2)$ or realistic noises will be investigated since the smallest deviation may be obtained by adding the different intensities of Gaussian noise.

Further, the results of comparison with the different number of measurements and different measurement ranges are indicated in Fig. 7(D). The expression $(\mathbf{N}_1 + 3\mathbf{N}_0)^*$ represents the results with 21 measurements. The expression $(\mathbf{N}_1 + 3\mathbf{N}_0)^{**}$ represents the results with 87 measurements. The expression $(\mathbf{N}_1 + 3\mathbf{N}_0)^+$ represents the results with the chosen measurement range of $1.0 \times 10^{-9} < \Theta < 1.6 \times 10^{-9}$. Indeed, increasing the num-

ber of measurements can further decrease the deviation of the mean value; however, it is undeniable that simply increasing the number of measurements can not decrease error bars. Even the error bar of the 87 measurements marked with $(\mathbf{N}_1 + 3\mathbf{N}_0)^{**}$ seems too large for estimation of the time delay τ . Nevertheless, when comparing the results $(\mathbf{N}_1 + 3\mathbf{N}_0)^+$ with the results $(\mathbf{N}_1 + 3\mathbf{N}_0)^{**}$, it can be found in Table IV that decreasing the measurement range $[\Theta_{\text{Min}}, \Theta_{\text{Max}}]$ can significantly reduce error bars but lead to small deviation of the mean value. There are two reasons why we set the measurement range $[\Theta_{\text{Min}}, \Theta_{\text{Max}}]$. Firstly, it is natural to set the minimum value Θ_{Min} and the maximum Θ_{Max} when a high enough resolution is required for estimation of the quality Θ in this paper, because the detector (APD and Scope) response is dominated by the saturation effect [19]. In addition, when the number of AD digits is determined, decreasing the measurement range $[\Theta_{\text{Min}}, \Theta_{\text{Max}}]$ can obtain higher resolution for estimation of the quality Θ [61]. Secondly, the theoretical measurement range can be pre-determined by discarding unreasonable measurement results. The unreasonable measurement results may be corresponding

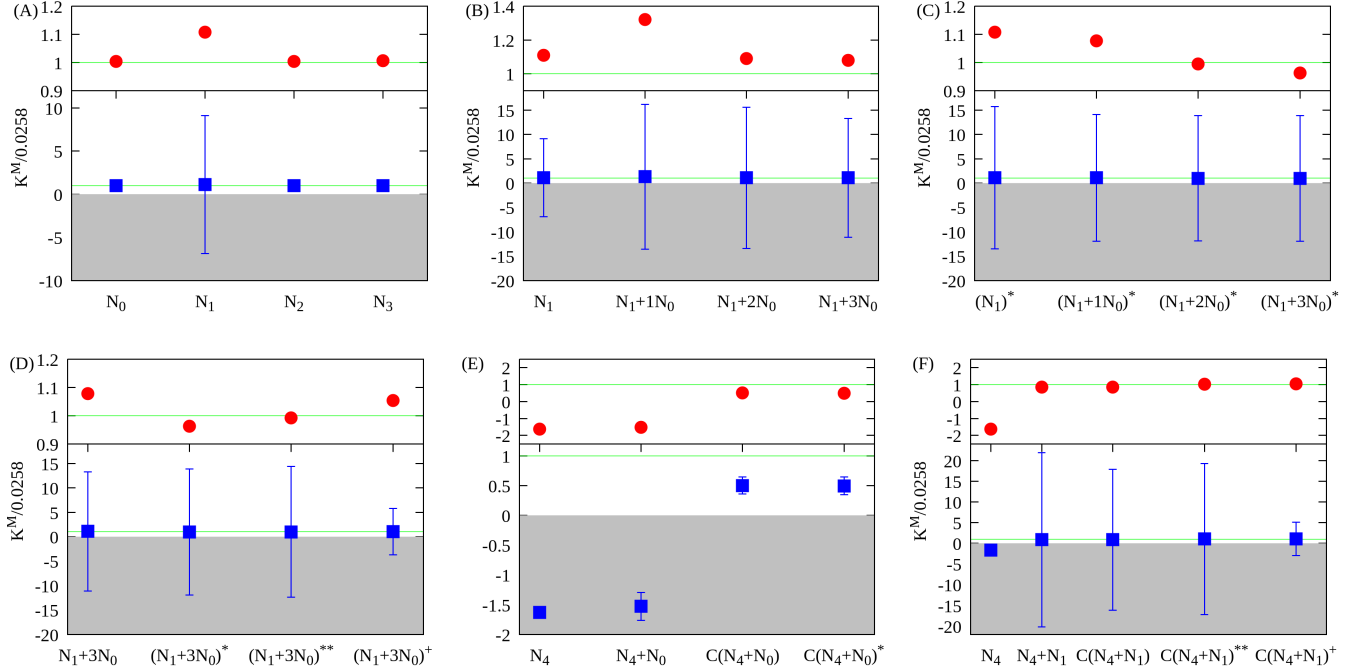


FIG. 7. The normalized sensitivity in the AWVA scheme under the various noises: (A) the results of 7 measurements under frequency-stationary noises; (B) the results of 7 measurements under the combination of Gaussian noises $\mathbf{N}_0(t)$ and $1/f$ noises $\mathbf{N}_1(t)$; (C) the results of 21 measurements with superscript “*” under the combination of Gaussian noises $\mathbf{N}_0(t)$ and $1/f$ noises $\mathbf{N}_1(t)$; (D) the results with different measurements and different measurement range under the combination of Gaussian noises $\mathbf{N}_0(t)$ and $1/f$ noises $\mathbf{N}_1(t)$; (E) the results of 7 measurements under the combination of Gaussian noises $\mathbf{N}_0(t)$ and frequency-nonstationary noises $\mathbf{N}_4(t)$; (F) the results of 7 measurements under the combination of $1/f$ noises $\mathbf{N}_1(t)$ and frequency-nonstationary noises $\mathbf{N}_4(t)$. The expression (...) represents the results with 21 measurements. The expression (...)** represents the results with 87 measurements. The expression (...) represents the results with the chosen measurement range of $1.0 \times 10^{-9} < \Theta < 1.6 \times 10^{-9}$. The expression C(...) represents the results with the voltage-clamp approach. The circular red data represent the mean value of the normalized sensitivity. The square blue data represent the mean value with error bars of the normalized sensitivity. The green line represents the theoretical value.

to results $\Theta(t)$ deviating far from the theoretical curves $\Theta_{\Pi}(t)$, because the robustness of one system with long-range measurement can not remain asymptotically stable all the time when the random disturbance to the system is very strong. In other words, the robustness characterized by error bars in our system and another system associated with generalized variance should be modeled and measured by inputting feasible range measurements. Similarly, a generic framework for modeling and measurement of process robustness in manufacturing system has been studied by starting with the necessary process: selecting a manufacturing process, identifying the input process parameters, response variables and their feasible range of operations (corresponding to the measurement range $[\Theta_{\text{Min}}, \Theta_{\text{Max}}]$ in this work) [62]. In addition, it is worth working for further studying and quantitatively calculating the process robustness of the AWVA scheme by following the generic framework in Ref. [62]. In a word, it is necessary and effective to set the feasible measurement range $[\Theta_{\text{Min}}, \Theta_{\text{Max}}]$ for obtaining a smaller error bar. Note that decreasing the measurement range leads to a larger deviation of the mean value in Fig. 7(D). This larger deviation is due to fewer valid measurements

and can be eliminated by further increasing the number of measurements.

In conclusion, the simulation results indicate that the low-frequency noise has an adverse impact on the AWVA measurements when the signal is also low frequency. The analysis provides a referable principle to perform the AWVA measurements, which is trying to ensure that the signal (initial pointer) is not in the same frequency band as the noise. At the very least, multiple measurements and dominating measurement range by adding additive Gaussian noise may enhance the precision of the AWVA technique under the low-frequency noise $\mathbf{N}_1(t, \sigma^2)$.

B. Effects of frequency-nonstationary noises

We further investigate more realistic and complex noises, namely the frequency-nonstationary noises $\mathbf{N}_4(t)$, $\mathbf{N}_{40}(t)$ and $\mathbf{N}_{41}(t)$, and in the next we call this kind of noise as “impulsive noise”. In this paper, impulsive noise $\mathbf{N}_4(t)$ is generated by a series of short Gaussian pulses, caused by a variety of sources, such as switching noise, adverse channel environments in a communication sys-

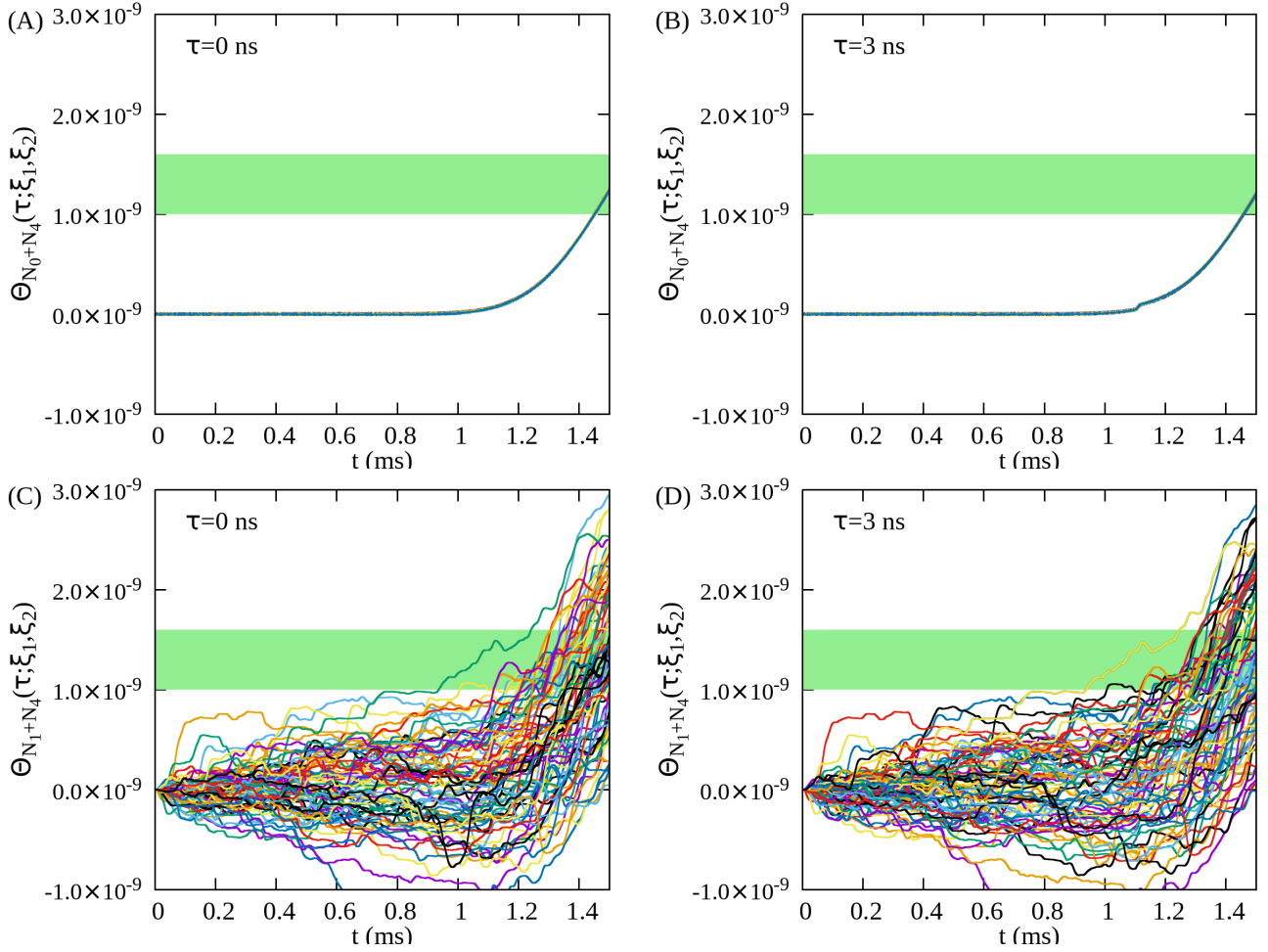


FIG. 8. Simulation result of $\Theta(\tau)$ with 21 measurements under noises $\mathbf{N}_{40}(t)$ (upper panels) and with 87 measurements under noises $\mathbf{N}_{41}(t)$ (lower panels). Subfigures (A) and (C) represent the results of measuring time delay $\tau = 0$ ns; Subfigures (B) and (D) represent the results of measuring time delay $\tau = 3$ ns. The green band represents the dominated measurement range of $1.0 \times 10^{-9} < \Theta < 1.6 \times 10^{-9}$. Lines in each subfigure represent the different measurements with various seed ξ_1 and ξ_2 . The data at $t = 1.5$ ms are displayed in Table V and Table VI.

tem, clicks from computer keyboards etc [60]. By adding these noises into the final signal I_1^{out} , some simulation results on Simulink are shown in Fig. 6, Fig. 8 Table I and Table VI.

Fig. 6 shows the simulation results with 7 measurements of the final signals $I_1^{out}(t)$, the auto-correlative intensity $\Theta(\tau = 0\text{ns})$ and $\Theta(\tau = 3\text{ns})$ under various impulsive noises. The simulation results under noises \mathbf{N}_4 and \mathbf{N}_{40} show a reduced sensitivity with smaller error bars. In other words, the results under noises \mathbf{N}_4 and \mathbf{N}_{40} do not give a valid result (corresponding to $K^M > 0$) even if the error bar is included. Also, the low-frequency noise $\mathbf{N}_1(t, \sigma^2)$ may weaken the effect of the impulsive noise $\mathbf{N}_4(t)$ on the AWVA measurements with positive sensitivity by ignoring the huge error bar. To summarize, the impulsive noise $\mathbf{N}_4(t)$ is worse than the low-frequency noise $\mathbf{N}_1(t, \sigma^2)$ and must be eliminated for achieving robustness in the AWVA scheme.

The standard method for removal of impulsive noise

is the median filter². However, the median filter often results in some signal degradation [60]. Therefore, we propose another simple and effective method, namely “voltage-clamp”, to suppress the impulsive noise $\mathbf{N}_4(t)$. On the one hand, “voltage-clamp” limiting the maximum of signals seems to be natural since the detector response is dominated by the saturation effect [19]. On the other hand, the analog clamp circuit has matured and is now widely used in other scientific fields[63, 64]. As shown in Table I, Fig. 7(E) and Fig. 7(F), the final signal $I_1^{out}(t)$ with the combination of noises $\mathbf{N}_4 + \mathbf{N}_0$ and $\mathbf{N}_4 + \mathbf{N}_1$ after clamping the maximum of signals at 2.0×10^{-4} are

² Median filtering is a kind of nonlinear signal processing technology that can effectively suppress noise based on sorting statistics theory. The basic principle of median filtering is to replace the value of a point in a digital sequence with the median value of each point in a neighborhood of the point so that the surrounding pixel value is close to the real value, to eliminate isolated noise points.

denoted as $C(I_1^{out} + \mathbf{N}_4 + \mathbf{N}_0)$ and $C(I_1^{out} + \mathbf{N}_4 + \mathbf{N}_1)$ respectively. Fig. 7(E) indicates that the measurements after clamping the final signals $C(I_1^{out} + \mathbf{N}_4 + \mathbf{N}_0)$ obtain more accurate results with positive sensitivity than the measurements under noise $\mathbf{N}_4 + \mathbf{N}_0$. In addition, increasing the number of measurements can not improve the precision of the AWVA measurement under noise $\mathbf{N}_{40}(t)$ in spite of the negligible error bar. The deviation of the statistical mean will not decrease as the number of the measurements increases, and this deviation seems to be a systematic error of the AWVA measurement under the certain noise $\mathbf{N}_{40}(t)$ in this paper. Note that setting the measurement range $1.0 \times 10^{-9} < \Theta < 1.6 \times 10^{-9}$ will not affect the precision since the value of $\Theta(t = 1.5\text{ms})$ naturally locate in this range as shown in Figs. 8(A) and 8(B).

At the same time for the measurement under $\mathbf{N}_4 + \mathbf{N}_1$ as shown in Fig. 7(F), clamping can optimize the measurement result with a smaller error bar. However, the error bar of the measurement $C(\mathbf{N}_4 + \mathbf{N}_1)$ is still too large for estimating time delay τ .

Another effective approach to reducing the error bar of the measurement $C(\mathbf{N}_4 + \mathbf{N}_1)$, as discussed in Sec. III A, is further adding the number of the measurement and dominating measurement range. Therefore, the simulation results of $\Theta(\tau)$ under the combination of Gaussian noises $\mathbf{N}_1(t)$ and impulsive noise $\mathbf{N}_4(t)$ are shown in Fig. 8. The data at $t=1.5$ ms are displayed in Table VI. The normalized sensitivity and error bar of the measurement $C(\mathbf{N}_4 + \mathbf{N}_1)^{**}$ and the measurement $C(\mathbf{N}_4 + \mathbf{N}_1)^+$ can be found in Table I. Predictably, Fig. 7F indicates that the error bar of measurement $C(\mathbf{N}_4 + \mathbf{N}_1)^+$ is sharply reduced when compared to the measurement $C(\mathbf{N}_4 + \mathbf{N}_1)$ and the measurement $C(\mathbf{N}_4 + \mathbf{N}_1)^{**}$.

In general, the AWVA measurements have the worst robustness under impulsive noise $\mathbf{N}_4(t)$. To be mitigate this, a measurement scheme with fewer measurements by adding the Gaussian noise and limiting the maximum of signals can effectively increase the precision with positive sensitivity and a smaller deviation of the mean value. In addition, another measurement scheme with a sufficient number of measurements by adding additive 1/f noise, clamping the signals, and further dominating measurement range can lead to a more precise value of statistical mean with a certain amount of error.

IV. SUMMARY

We have investigated the influence of non-Gaussian noises on auto-correlative weak-value amplification (AWVA) for precision phase estimation. Simulated measurements on Simulink for estimating the time shift have been derived under various noises. In this paper, two types of noise, frequency-stationary noises, and frequency-nonstationary noises were studied. Specifically, low frequency (1/f) noise, medium frequency noise, high-frequency noise, and the combination of these noises and the Gaussian noise were chosen as a proxy for the

measurements under frequency-stationary noises. In addition, the impulsive noise and the mixed noise of the impulsive noise and Gaussian noise or low frequency (1/f) noise were studied as representative examples of the measurements under the frequency-nonstationary noises.

According to the results of the simulation experiment, we obtained the following conclusions: 1) Low-frequency noise has a greater adverse impact on the AWVA measurements than other frequency-stationary noises due to the coincidence of the noises and signals in the frequency domain. 2) Precise characterization of the technique and environmental noises can provide a selection of initial pointers to avoid the coincidence of the noises and signals in the frequency domain. 3) The frequency-nonstationary noises, such as impulsive noise, maybe the worst kind of noise and lead to wrong (negativity sensitivity) measurements. 4) Increasing the number of measurements, adding additive frequency-stationary noise, limiting the maximum value of the detected signals, and dominating the measurement range may have the potential to improve the precision of the AWVA technique under the worst noises with both the smaller deviation of the mean value and the smaller error bar. Note that the multiple measurements with these complex data processing may make measurement difficult and inconvenient. It is worth to further adding the field-programmable gate array (FPGA) in electronics [65–67] to the WVA scheme for logic controls optical components and real-time data processing.

Our simulation of the AWVA measurements under more realistic/complex noises rather than Gaussian noises [43] further demonstrates that the robustness of the AWVA technique can resist environmental and instrument disturbances.

ACKNOWLEDGMENTS

This study is supported by the National Science Foundation of China (No. 41630317), MOST Special Fund from the State Key Laboratory of Geological Processes and Mineral Resources, the China University of Geosciences (No. MSFGPMR01-4). J-H. H. acknowledges support from the China Scholarship Council (CSC No. 202206410063). A.C.D. acknowledges support from the EPSRC, Impact Acceleration Account (EP/R511705/1).

TABLE II. Parameters and some characteristic numerical results of measuring time shift $\tau = 3.0 \times 10^{-9}$ under frequency-stationary noises with SNR= -5.3 dB in the AWVA scheme. The quantity Θ_0 and Θ_τ are measured at $t = 1.5$ ms. $\mathbf{N}(\xi)$ with various ξ represent the multiple measurements with the different initial times.

Noise	$\mathbf{N}(t, \xi_1)$	$\mathbf{N}(t, \xi_2)$	Θ_0	Θ_τ	$\bar{\Theta}_0$	$\bar{\Theta}_\tau$
-	-	-	1.2442×10^{-9}	1.1666×10^{-9}		
\mathbf{N}_0	$\xi_1=126$	$\xi_2=913$	1.2514×10^{-9}	1.1734×10^{-9}		
	$\xi_1=632$	$\xi_2=097$	1.2484×10^{-9}	1.1709×10^{-9}		
	$\xi_1=278$	$\xi_2=546$	1.2374×10^{-9}	1.1597×10^{-9}	1.2459×10^{-9}	1.1682×10^{-9}
	$\xi_1=957$	$\xi_2=964$	1.2451×10^{-9}	1.1678×10^{-9}	$\pm 0.0048 \times 10^{-9}$	$\pm 0.0047 \times 10^{-9}$
	$\xi_1=157$	$\xi_2=970$	1.2472×10^{-9}	1.1694×10^{-9}		
	$\xi_1=485$	$\xi_2=800$	1.2498×10^{-9}	1.1720×10^{-9}		
	$\xi_1=141$	$\xi_2=421$	1.2422×10^{-9}	1.1647×10^{-9}		
\mathbf{N}_1	$\xi_1=915$	$\xi_2=792$	1.2418×10^{-9}	1.1322×10^{-9}		
	$\xi_1=959$	$\xi_2=655$	1.1444×10^{-9}	1.0713×10^{-9}		
	$\xi_1=035$	$\xi_2=849$	1.5659×10^{-9}	1.4780×10^{-9}	1.3066×10^{-9}	1.2208×10^{-9}
	$\xi_1=933$	$\xi_2=678$	1.7368×10^{-9}	1.6829×10^{-9}	$\pm 0.3047 \times 10^{-9}$	$\pm 0.3144 \times 10^{-9}$
	$\xi_1=757$	$\xi_2=743$	1.4272×10^{-9}	1.3351×10^{-9}		
	$\xi_1=392$	$\xi_2=655$	1.2277×10^{-9}	1.1390×10^{-9}		
	$\xi_1=171$	$\xi_2=706$	0.8029×10^{-9}	0.7074×10^{-9}		
\mathbf{N}_2	$\xi_1=031$	$\xi_2=276$	1.2500×10^{-9}	1.1723×10^{-9}		
	$\xi_1=046$	$\xi_2=097$	1.2520×10^{-9}	1.1744×10^{-9}		
	$\xi_1=823$	$\xi_2=694$	1.2280×10^{-9}	1.1503×10^{-9}	1.2399×10^{-9}	1.1622×10^{-9}
	$\xi_1=317$	$\xi_2=950$	1.2405×10^{-9}	1.1628×10^{-9}	$\pm 0.0153 \times 10^{-9}$	$\pm 0.0153 \times 10^{-9}$
	$\xi_1=034$	$\xi_2=438$	1.2571×10^{-9}	1.1794×10^{-9}		
	$\xi_1=381$	$\xi_2=765$	1.2391×10^{-9}	1.1614×10^{-9}		
	$\xi_1=795$	$\xi_2=718$	1.2129×10^{-9}	1.1352×10^{-9}		
\mathbf{N}_3	$\xi_1=489$	$\xi_2=445$	1.2495×10^{-9}	1.1718×10^{-9}		
	$\xi_1=646$	$\xi_2=709$	1.2506×10^{-9}	1.1730×10^{-9}		
	$\xi_1=754$	$\xi_2=267$	1.2418×10^{-9}	1.1641×10^{-9}	1.2456×10^{-9}	1.1677×10^{-9}
	$\xi_1=679$	$\xi_2=655$	1.2447×10^{-9}	1.1670×10^{-9}	$\pm 0.0034 \times 10^{-9}$	$\pm 0.0035 \times 10^{-9}$
	$\xi_1=112$	$\xi_2=168$	1.2454×10^{-9}	1.1677×10^{-9}		
	$\xi_1=498$	$\xi_2=959$	1.2455×10^{-9}	1.1668×10^{-9}		
	$\xi_1=344$	$\xi_2=585$	1.2417×10^{-9}	1.1640×10^{-9}		
$\mathbf{N}_1(\xi_1)+\mathbf{N}_0(\xi'_1 = 223)$ $\mathbf{N}_1(\xi_2)+\mathbf{N}_0(\xi'_1 = 751)$	$\xi_1=255$	$\xi_2=505$	1.3636×10^{-9}	1.2990×10^{-9}		
	$\xi_1=699$	$\xi_2=890$	1.3549×10^{-9}	1.2664×10^{-9}		
	$\xi_1=547$	$\xi_2=138$	2.2325×10^{-9}	2.1146×10^{-9}	1.5114×10^{-9}	1.4091×10^{-9}
	$\xi_1=149$	$\xi_2=257$	2.2083×10^{-9}	1.9833×10^{-9}	$\pm 0.5998 \times 10^{-9}$	$\pm 0.5516 \times 10^{-9}$
	$\xi_1=840$	$\xi_2=254$	1.6924×10^{-9}	1.5661×10^{-9}		
	$\xi_1=814$	$\xi_2=243$	1.2082×10^{-9}	1.1642×10^{-9}		
$\mathbf{N}_1(\xi_1)+2\mathbf{N}_0(\xi'_1 = 223)$ $\mathbf{N}_1(\xi_2)+2\mathbf{N}_0(\xi'_1 = 751)$	$\xi_1=255$	$\xi_2=505$	1.3358×10^{-9}	1.2716×10^{-9}		
	$\xi_1=699$	$\xi_2=890$	1.3337×10^{-9}	1.2458×10^{-9}		
	$\xi_1=547$	$\xi_2=138$	2.2123×10^{-9}	2.0950×10^{-9}	1.4664×10^{-9}	1.3825×10^{-9}
	$\xi_1=149$	$\xi_2=257$	2.0440×10^{-9}	1.9446×10^{-9}	$\pm 0.5742 \times 10^{-9}$	$\pm 0.5488 \times 10^{-9}$
	$\xi_1=840$	$\xi_2=254$	1.6571×10^{-9}	1.5313×10^{-9}		
	$\xi_1=814$	$\xi_2=243$	1.1843×10^{-9}	1.1408×10^{-9}		
	$\xi_1=929$	$\xi_2=349$	0.4980×10^{-9}	0.4485×10^{-9}		

TABLE III. Parameters and some characteristic numerical results of measuring time shift $\tau = 3.0 \times 10^{-9}$ under noises $\mathbf{N}_1(\xi)$, $\mathbf{N}_1(\xi) + 1\mathbf{N}_0(\xi)$ and $\mathbf{N}_1(\xi) + 3\mathbf{N}_0(\xi)$ with 21 measurements.

Noise	$\mathbf{N}(t, \xi_1)$	$\mathbf{N}(t, \xi_2)$	Θ_0	Θ_τ	$\bar{\Theta}_0$	$\bar{\Theta}_\tau$
\mathbf{N}_1	$\xi_1=106$	$\xi_2=442$	0.5840×10^{-9}	0.5176×10^{-9}		
	$\xi_1=961$	$\xi_2=004$	2.6224×10^{-9}	2.5338×10^{-9}		
	$\xi_1=774$	$\xi_2=817$	0.6769×10^{-9}	0.6053×10^{-9}		
	$\xi_1=868$	$\xi_2=084$	1.0751×10^{-9}	1.0263×10^{-9}		
	$\xi_1=399$	$\xi_2=259$	1.7033×10^{-9}	1.6227×10^{-9}		
	$\xi_1=800$	$\xi_2=431$	0.8600×10^{-9}	0.7520×10^{-9}		
	$\xi_1=910$	$\xi_2=181$	1.1575×10^{-9}	1.0371×10^{-9}		
	$\xi_1=601$	$\xi_2=262$	2.4187×10^{-9}	2.2865×10^{-9}		
	$\xi_1=654$	$\xi_2=689$	0.5739×10^{-9}	0.5184×10^{-9}		
	$\xi_1=748$	$\xi_2=450$	1.4509×10^{-9}	1.3691×10^{-9}	1.4087×10^{-9}	1.3227×10^{-9}
	$\xi_1=083$	$\xi_2=228$	1.6167×10^{-9}	1.5671×10^{-9}	$\pm 0.5695 \times 10^{-9}$	$\pm 0.5621 \times 10^{-9}$
	$\xi_1=913$	$\xi_2=152$	2.1642×10^{-9}	2.0656×10^{-9}		
	$\xi_1=852$	$\xi_2=538$	1.8591×10^{-9}	1.7529×10^{-9}		
	$\xi_1=996$	$\xi_2=078$	1.6745×10^{-9}	1.5782×10^{-9}		
	$\xi_1=915$	$\xi_2=792$	1.2418×10^{-9}	1.1322×10^{-9}		
	$\xi_1=959$	$\xi_2=655$	1.1444×10^{-9}	1.0713×10^{-9}		
	$\xi_1=035$	$\xi_2=849$	1.5659×10^{-9}	1.4780×10^{-9}		
	$\xi_1=933$	$\xi_2=678$	1.7368×10^{-9}	1.6829×10^{-9}		
	$\xi_1=757$	$\xi_2=743$	1.4272×10^{-9}	1.3351×10^{-9}		
	$\xi_1=392$	$\xi_2=655$	1.2277×10^{-9}	1.1390×10^{-9}		
	$\xi_1=171$	$\xi_2=706$	0.8029×10^{-9}	0.7074×10^{-9}		
$\mathbf{N}_1(\xi_1)+\mathbf{N}_0(\xi'_1 = 223)$ $\mathbf{N}_1(\xi_2)+\mathbf{N}_0(\xi'_1 = 751)$	$\xi_1=145$	$\xi_2=136$	1.2186×10^{-9}	1.1499×10^{-9}		
	$\xi_1=859$	$\xi_2=579$	1.3178×10^{-9}	1.2307×10^{-9}		
	$\xi_1=549$	$\xi_2=144$	0.7085×10^{-9}	0.5998×10^{-9}		
	$\xi_1=853$	$\xi_2=622$	1.0090×10^{-9}	0.9109×10^{-9}		
	$\xi_1=350$	$\xi_2=513$	0.7453×10^{-9}	0.6595×10^{-9}		
	$\xi_1=401$	$\xi_2=075$	0.8513×10^{-9}	0.7704×10^{-9}		
	$\xi_1=239$	$\xi_2=123$	0.4524×10^{-9}	0.3976×10^{-9}		
	$\xi_1=189$	$\xi_2=239$	0.7542×10^{-9}	0.7104×10^{-9}		
	$\xi_1=417$	$\xi_2=049$	1.7368×10^{-9}	1.6687×10^{-9}		
	$\xi_1=902$	$\xi_2=944$	1.0811×10^{-9}	0.9862×10^{-9}	1.1465×10^{-9}	1.0631×10^{-9}
	$\xi_1=489$	$\xi_2=337$	0.3592×10^{-9}	0.2664×10^{-9}	$\pm 0.5171 \times 10^{-9}$	$\pm 0.4931 \times 10^{-9}$
	$\xi_1=900$	$\xi_2=369$	1.3852×10^{-9}	1.2852×10^{-9}		
	$\xi_1=111$	$\xi_2=780$	1.0228×10^{-9}	0.9786×10^{-9}		
	$\xi_1=389$	$\xi_2=241$	0.8557×10^{-9}	0.8475×10^{-9}		
	$\xi_1=255$	$\xi_2=505$	1.3636×10^{-9}	1.2990×10^{-9}		
	$\xi_1=699$	$\xi_2=890$	1.3549×10^{-9}	1.2664×10^{-9}		
	$\xi_1=547$	$\xi_2=138$	2.2325×10^{-9}	2.1146×10^{-9}		
	$\xi_1=149$	$\xi_2=257$	2.2083×10^{-9}	1.9833×10^{-9}		
	$\xi_1=840$	$\xi_2=254$	1.6924×10^{-9}	1.5661×10^{-9}		
	$\xi_1=814$	$\xi_2=243$	1.2082×10^{-9}	1.1642×10^{-9}		
	$\xi_1=929$	$\xi_2=349$	0.5203×10^{-9}	0.4703×10^{-9}		

Noise	$\mathbf{N}(t, \xi_1)$	$\mathbf{N}(t, \xi_2)$	Θ_0	Θ_τ	$\bar{\Theta}_0$	$\bar{\Theta}_\tau$
	$\xi_1=145$	$\xi_2=136$	1.1916×10^{-9}	1.1235×10^{-9}		
	$\xi_1=859$	$\xi_2=579$	1.3020×10^{-9}	1.2155×10^{-9}		
	$\xi_1=549$	$\xi_2=144$	0.6748×10^{-9}	0.5667×10^{-9}		
	$\xi_1=853$	$\xi_2=622$	0.9561×10^{-9}	0.8585×10^{-9}		
	$\xi_1=350$	$\xi_2=513$	0.7172×10^{-9}	0.6319×10^{-9}		
	$\xi_1=401$	$\xi_2=075$	0.8298×10^{-9}	0.7494×10^{-9}		
	$\xi_1=239$	$\xi_2=123$	0.4282×10^{-9}	0.3739×10^{-9}		
	$\xi_1=189$	$\xi_2=239$	0.7213×10^{-9}	0.6780×10^{-9}		
	$\xi_1=417$	$\xi_2=049$	1.7124×10^{-9}	1.6448×10^{-9}		
$\mathbf{N}_1(\xi_1)+2\mathbf{N}_0(\xi'_1 = 223)$	$\xi_1=902$	$\xi_2=944$	1.0543×10^{-9}	0.9600×10^{-9}	1.1124×10^{-9}	1.0354×10^{-9}
$\mathbf{N}_1(\xi_1)+2\mathbf{N}_0(\xi'_1 = 751)$	$\xi_1=489$	$\xi_2=337$	0.3369×10^{-9}	0.2447×10^{-9}	$\pm 0.5041 \times 10^{-9}$	$\pm 0.4924 \times 10^{-9}$
	$\xi_1=900$	$\xi_2=369$	1.3476×10^{-9}	1.2487×10^{-9}		
	$\xi_1=111$	$\xi_2=780$	0.9850×10^{-9}	0.9413×10^{-9}		
	$\xi_1=389$	$\xi_2=241$	0.8381×10^{-9}	0.8304×10^{-9}		
	$\xi_1=255$	$\xi_2=505$	1.3358×10^{-9}	1.2716×10^{-9}		
	$\xi_1=699$	$\xi_2=890$	1.3337×10^{-9}	1.2458×10^{-9}		
	$\xi_1=547$	$\xi_2=138$	2.2123×10^{-9}	2.0950×10^{-9}		
	$\xi_1=149$	$\xi_2=257$	2.0440×10^{-9}	1.9446×10^{-9}		
	$\xi_1=840$	$\xi_2=254$	1.6571×10^{-9}	1.5313×10^{-9}		
	$\xi_1=814$	$\xi_2=243$	1.1843×10^{-9}	1.1408×10^{-9}		
	$\xi_1=929$	$\xi_2=349$	0.4980×10^{-9}	0.4485×10^{-9}		
	$\xi_1=145$	$\xi_2=136$	1.1537×10^{-9}	1.0860×10^{-9}		
	$\xi_1=859$	$\xi_2=579$	1.2752×10^{-9}	1.1892×10^{-9}		
	$\xi_1=549$	$\xi_2=144$	0.6301×10^{-9}	0.5224×10^{-9}		
	$\xi_1=853$	$\xi_2=622$	0.8921×10^{-9}	0.7950×10^{-9}		
	$\xi_1=350$	$\xi_2=513$	0.6780×10^{-9}	0.5932×10^{-9}		
	$\xi_1=401$	$\xi_2=075$	0.7971×10^{-9}	0.7173×10^{-9}		
	$\xi_1=239$	$\xi_2=123$	0.3630×10^{-9}	0.3392×10^{-9}		
	$\xi_1=189$	$\xi_2=239$	0.6773×10^{-9}	0.6346×10^{-9}		
	$\xi_1=417$	$\xi_2=049$	1.6769×10^{-9}	1.6098×10^{-9}		
$\mathbf{N}_1(\xi_1)+3\mathbf{N}_0(\xi'_1 = 223)$	$\xi_1=902$	$\xi_2=944$	1.0166×10^{-9}	0.9228×10^{-9}	1.0717×10^{-9}	0.9966×10^{-9}
$\mathbf{N}_1(\xi_2)+3\mathbf{N}_0(\xi'_1 = 751)$	$\xi_1=489$	$\xi_2=337$	0.3036×10^{-9}	0.2118×10^{-9}	$\pm 0.5056 \times 10^{-9}$	$\pm 0.4919 \times 10^{-9}$
	$\xi_1=900$	$\xi_2=369$	1.2990×10^{-9}	1.2000×10^{-9}		
	$\xi_1=111$	$\xi_2=780$	0.9361×10^{-9}	0.8930×10^{-9}		
	$\xi_1=389$	$\xi_2=241$	0.8094×10^{-9}	0.8022×10^{-9}		
	$\xi_1=255$	$\xi_2=505$	1.2968×10^{-9}	1.2332×10^{-9}		
	$\xi_1=699$	$\xi_2=890$	1.3015×10^{-9}	1.2141×10^{-9}		
	$\xi_1=547$	$\xi_2=138$	2.1812×10^{-9}	2.0644×10^{-9}		
	$\xi_1=149$	$\xi_2=257$	1.9946×10^{-9}	1.8948×10^{-9}		
	$\xi_1=840$	$\xi_2=254$	1.6107×10^{-9}	1.4855×10^{-9}		
	$\xi_1=814$	$\xi_2=243$	1.1493×10^{-9}	1.1063×10^{-9}		
	$\xi_1=929$	$\xi_2=349$	0.4646×10^{-9}	0.4157×10^{-9}		

TABLE IV. Parameters and results under noises $\mathbf{N}_1(\xi_1) + 3\mathbf{N}_0(\xi'_1 = 223)$ and $\mathbf{N}_1(\xi_2) + 3\mathbf{N}_0(\xi'_2 = 751)$. Blue data are results with the chosen measurement range of $1.0 \times 10^{-9} < \Theta < 1.6 \times 10^{-9}$.

$\mathbf{N}(t, \xi_1)$	$\mathbf{N}(t, \xi_2)$	Θ_0	Θ_τ
$\xi_1=145$	$\xi_2=136$	1.1537×10^{-9}	1.0860×10^{-9}
$\xi_1=859$	$\xi_2=579$	1.2752×10^{-9}	1.1892×10^{-9}
$\xi_1=549$	$\xi_2=144$	0.6301×10^{-9}	0.5224×10^{-9}
$\xi_1=853$	$\xi_2=622$	0.8921×10^{-9}	0.7950×10^{-9}
$\xi_1=350$	$\xi_2=513$	0.6780×10^{-9}	0.5932×10^{-9}
$\xi_1=401$	$\xi_2=075$	0.7971×10^{-9}	0.7173×10^{-9}
$\xi_1=239$	$\xi_2=123$	0.3630×10^{-9}	0.3392×10^{-9}
$\xi_1=189$	$\xi_2=239$	0.6773×10^{-9}	0.6346×10^{-9}
$\xi_1=417$	$\xi_2=049$	1.6769×10^{-9}	1.6098×10^{-9}
$\xi_1=902$	$\xi_2=944$	1.0166×10^{-9}	0.9228×10^{-9}
$\xi_1=489$	$\xi_2=337$	0.3036×10^{-9}	0.2118×10^{-9}
$\xi_1=900$	$\xi_2=369$	1.2990×10^{-9}	1.2000×10^{-9}
$\xi_1=111$	$\xi_2=780$	0.9361×10^{-9}	0.8930×10^{-9}
$\xi_1=389$	$\xi_2=241$	0.8094×10^{-9}	0.8022×10^{-9}
$\xi_1=255$	$\xi_2=505$	1.2968×10^{-9}	1.2332×10^{-9}
$\xi_1=699$	$\xi_2=890$	1.3015×10^{-9}	1.2141×10^{-9}
$\xi_1=547$	$\xi_2=138$	2.1812×10^{-9}	2.0644×10^{-9}
$\xi_1=149$	$\xi_2=257$	1.9946×10^{-9}	1.8948×10^{-9}
$\xi_1=840$	$\xi_2=254$	1.6107×10^{-9}	1.4855×10^{-9}
$\xi_1=814$	$\xi_2=243$	1.1493×10^{-9}	1.1063×10^{-9}
$\xi_1=929$	$\xi_2=349$	0.4646×10^{-9}	0.4157×10^{-9}
$\xi_1=815$	$\xi_2=127$	1.0301×10^{-9}	0.9384×10^{-9}
$\xi_1=906$	$\xi_2=914$	0.8587×10^{-9}	0.7678×10^{-9}
$\xi_1=633$	$\xi_2=279$	2.1003×10^{-9}	2.0566×10^{-9}
$\xi_1=098$	$\xi_2=547$	1.5072×10^{-9}	1.4217×10^{-9}
$\xi_1=486$	$\xi_2=142$	1.5166×10^{-9}	1.4541×10^{-9}
$\xi_1=422$	$\xi_2=793$	1.2140×10^{-9}	1.1585×10^{-9}
$\xi_1=656$	$\xi_2=850$	1.4726×10^{-9}	1.2332×10^{-9}
$\xi_1=758$	$\xi_2=393$	0.9281×10^{-9}	0.8948×10^{-9}
$\xi_1=172$	$\xi_2=032$	0.8067×10^{-9}	0.7063×10^{-9}
$\xi_1=277$	$\xi_2=098$	0.8474×10^{-9}	0.7157×10^{-9}
$\xi_1=695$	$\xi_2=951$	1.0869×10^{-9}	0.9946×10^{-9}
$\xi_1=317$	$\xi_2=035$	0.8198×10^{-9}	0.7831×10^{-9}
$\xi_1=439$	$\xi_2=766$	1.9543×10^{-9}	1.9114×10^{-9}
$\xi_1=382$	$\xi_2=796$	1.4791×10^{-9}	1.3924×10^{-9}
$\xi_1=496$	$\xi_2=647$	1.4676×10^{-9}	1.4054×10^{-9}
$\xi_1=710$	$\xi_2=277$	1.1536×10^{-9}	1.0985×10^{-9}
$\xi_1=656$	$\xi_2=119$	1.4924×10^{-9}	1.4007×10^{-9}
$\xi_1=960$	$\xi_2=586$	0.7670×10^{-9}	0.6741×10^{-9}
$\xi_1=341$	$\xi_2=224$	0.8957×10^{-9}	0.8098×10^{-9}
$\xi_1=752$	$\xi_2=506$	2.5663×10^{-9}	2.5013×10^{-9}
$\xi_1=256$	$\xi_2=700$	0.8236×10^{-9}	0.7385×10^{-9}
$\xi_1=891$	$\xi_2=548$	0.8674×10^{-9}	0.8270×10^{-9}
$\xi_1=150$	$\xi_2=841$	1.0504×10^{-9}	0.9590×10^{-9}
$\xi_1=258$	$\xi_2=255$	0.7360×10^{-9}	0.6462×10^{-9}

$\mathbf{N}(t, \xi_1)$	$\mathbf{N}(t, \xi_2)$	Θ_0	Θ_τ
$\xi_1=815$	$\xi_2=930$	1.9715×10^{-9}	1.9271×10^{-9}
$\xi_1=244$	$\xi_2=350$	1.5036×10^{-9}	1.4185×10^{-9}
$\xi_1=252$	$\xi_2=474$	1.5152×10^{-9}	1.4534×10^{-9}
$\xi_1=258$	$\xi_2=586$	1.1929×10^{-9}	1.1385×10^{-9}
$\xi_1=918$	$\xi_2=758$	1.5201×10^{-9}	1.4272×10^{-9}
$\xi_1=381$	$\xi_2=076$	0.6953×10^{-9}	0.6019×10^{-9}
$\xi_1=568$	$\xi_2=054$	0.9418×10^{-9}	0.8558×10^{-9}
$\xi_1=531$	$\xi_2=935$	2.5270×10^{-9}	2.4604×10^{-9}
$\xi_1=780$	$\xi_2=130$	0.8408×10^{-9}	0.7554×10^{-9}
$\xi_1=891$	$\xi_2=548$	0.8674×10^{-9}	0.8270×10^{-9}
$\xi_1=163$	$\xi_2=312$	0.9864×10^{-9}	0.8947×10^{-9}
$\xi_1=795$	$\xi_2=529$	0.7323×10^{-9}	0.6424×10^{-9}
$\xi_1=166$	$\xi_2=263$	2.0035×10^{-9}	1.9610×10^{-9}
$\xi_1=602$	$\xi_2=655$	1.5406×10^{-9}	1.4554×10^{-9}
$\xi_1=749$	$\xi_2=084$	1.4693×10^{-9}	1.4078×10^{-9}
$\xi_1=229$	$\xi_2=153$	1.2322×10^{-9}	1.1770×10^{-9}
$\xi_1=539$	$\xi_2=079$	1.5088×10^{-9}	1.4154×10^{-9}
$\xi_1=997$	$\xi_2=443$	0.8252×10^{-9}	0.7318×10^{-9}
$\xi_1=107$	$\xi_2=005$	0.9672×10^{-9}	0.8801×10^{-9}
$\xi_1=982$	$\xi_2=776$	2.4840×10^{-9}	2.4171×10^{-9}
$\xi_1=818$	$\xi_2=085$	0.7937×10^{-9}	0.7076×10^{-9}
$\xi_1=869$	$\xi_2=400$	0.8002×10^{-9}	0.7587×10^{-9}
$\xi_1=260$	$\xi_2=432$	1.1482×10^{-9}	1.0569×10^{-9}
$\xi_1=801$	$\xi_2=911$	0.7959×10^{-9}	0.7051×10^{-9}
$\xi_1=182$	$\xi_2=146$	1.9713×10^{-9}	1.9281×10^{-9}
$\xi_1=264$	$\xi_2=137$	1.5807×10^{-9}	1.4951×10^{-9}
$\xi_1=580$	$\xi_2=145$	1.4884×10^{-9}	1.4261×10^{-9}
$\xi_1=854$	$\xi_2=351$	1.2621×10^{-9}	1.2066×10^{-9}
$\xi_1=402$	$\xi_2=240$	1.5174×10^{-9}	1.4239×10^{-9}
$\xi_1=184$	$\xi_2=418$	0.7976×10^{-9}	0.7046×10^{-9}
$\xi_1=240$	$\xi_2=050$	0.8582×10^{-9}	0.7712×10^{-9}
$\xi_1=903$	$\xi_2=491$	2.4560×10^{-9}	2.3901×10^{-9}
$\xi_1=945$	$\xi_2=490$	0.8582×10^{-9}	0.7545×10^{-9}
$\xi_1=338$	$\xi_2=370$	0.8885×10^{-9}	0.8460×10^{-9}
$\xi_1=781$	$\xi_2=242$	1.5364×10^{-9}	1.4449×10^{-9}
$\xi_1=097$	$\xi_2=943$	0.8137×10^{-9}	0.7199×10^{-9}
$\xi_1=132$	$\xi_2=957$	0.9510×10^{-9}	0.8645×10^{-9}
$\xi_1=576$	$\xi_2=235$	2.5337×10^{-9}	2.4687×10^{-9}
$\xi_1=060$	$\xi_2=354$	0.7401×10^{-9}	0.6554×10^{-9}
$\xi_1=822$	$\xi_2=044$	0.8344×10^{-9}	0.7939×10^{-9}
$\xi_1=650$	$\xi_2=248$	1.3710×10^{-9}	1.2784×10^{-9}
$\xi_1=548$	$\xi_2=745$	0.7917×10^{-9}	0.6990×10^{-9}
Θ_{Min}	Θ_{Max}	$\bar{\Theta}_0$	$\bar{\Theta}_\tau$
0.0×10^{-9}	3.0×10^{-9}	1.2247×10^{-9}	1.1479×10^{-9}
		$\pm 0.5173 \times 10^{-9}$	$\pm 0.5190 \times 10^{-9}$
1.0×10^{-9}	1.6×10^{-9}	1.3537×10^{-9}	1.2718×10^{-9}
		$\pm 0.1846 \times 10^{-9}$	$\pm 0.1830 \times 10^{-9}$

TABLE V. Parameters and some characteristic results under frequency-nonstationary noises.

Noise	$\mathbf{N}(t, \xi_1)$	$\mathbf{N}(t, \xi_2)$	Θ_0	Θ_τ	$\bar{\Theta}_0$	$\bar{\Theta}_\tau$	
\mathbf{N}_4	-	-	1.2443×10^{-9}	1.3707×10^{-9}			
$\mathbf{N}_4 + \mathbf{N}_0(\xi_1)$	$\xi_1=196$	$\xi_2=251$	1.2454×10^{-9}	1.3670×10^{-9}			
	$\xi_1=616$	$\xi_2=473$	1.2486×10^{-9}	1.3829×10^{-9}			
	$\xi_1=351$	$\xi_2=830$	1.2402×10^{-9}	1.3692×10^{-9}	1.2473×10^{-9}	1.3683×10^{-9}	
	$\mathbf{N}_4 + \mathbf{N}_0(\xi_2)$	$\xi_1=585$	$\xi_2=549$	1.2506×10^{-9}	1.3761×10^{-9}	$\pm 0.0054 \times 10^{-9}$	$\pm 0.0131 \times 10^{-9}$
	$\xi_1=917$	$\xi_2=285$	1.2407×10^{-9}	1.3423×10^{-9}			
	$\xi_1=757$	$\xi_2=753$	1.2537×10^{-9}	1.3761×10^{-9}			
	$\xi_1=380$	$\xi_2=567$	1.2522×10^{-9}	1.3647×10^{-9}			
$\mathbf{N}_4 + \mathbf{N}_1(\xi_1)$	$\xi_1=053$	$\xi_2=530$	1.4505×10^{-9}	1.3681×10^{-9}			
	$\xi_1=799$	$\xi_2=934$	2.3359×10^{-9}	2.2737×10^{-9}			
	$\xi_1=129$	$\xi_2=568$	2.1001×10^{-9}	2.0324×10^{-9}	1.4008×10^{-9}	1.3347×10^{-9}	
	$\mathbf{N}_4 + \mathbf{N}_1(\xi_2)$	$\xi_1=469$	$\xi_2=011$	1.4895×10^{-9}	1.4000×10^{-9}	$\pm 0.8167 \times 10^{-9}$	$\pm 0.8104 \times 10^{-9}$
	$\xi_1=337$	$\xi_2=162$	1.6610×10^{-9}	1.5972×10^{-9}			
	$\xi_1=704$	$\xi_2=311$	-0.1131×10^{-9}	-0.1653×10^{-9}			
	$\xi_1=528$	$\xi_2=165$	0.8819×10^{-9}	0.8368×10^{-9}			
$\mathbf{C}(\mathbf{N}_4 + \mathbf{N}_0(\xi_1))$	$\xi_1=196$	$\xi_2=251$	1.2454×10^{-9}	1.2065×10^{-9}			
	$\xi_1=616$	$\xi_2=473$	1.2486×10^{-9}	1.2120×10^{-9}			
	$\xi_1=351$	$\xi_2=830$	1.2402×10^{-9}	1.2018×10^{-9}	1.2473×10^{-9}	1.2085×10^{-9}	
	$\mathbf{C}(\mathbf{N}_4 + \mathbf{N}_0(\xi_2))$	$\xi_1=585$	$\xi_2=549$	1.2506×10^{-9}	1.2120×10^{-9}	$\pm 0.0054 \times 10^{-9}$	$\pm 0.0058 \times 10^{-9}$
	$\xi_1=917$	$\xi_2=285$	1.2407×10^{-9}	1.1998×10^{-9}			
	$\xi_1=757$	$\xi_2=753$	1.2537×10^{-9}	1.2153×10^{-9}			
	$\xi_1=380$	$\xi_2=567$	1.2522×10^{-9}	1.2121×10^{-9}			
$\mathbf{C}(\mathbf{N}_4 + \mathbf{N}_1(\xi_1))$	$\xi_1=053$	$\xi_2=530$	1.2193×10^{-9}	1.1369×10^{-9}			
	$\xi_1=799$	$\xi_2=934$	2.2048×10^{-9}	2.1426×10^{-9}			
	$\xi_1=129$	$\xi_2=568$	1.8539×10^{-9}	1.7862×10^{-9}	1.3242×10^{-9}	1.2586×10^{-9}	
	$\mathbf{C}(\mathbf{N}_4 + \mathbf{N}_1(\xi_2))$	$\xi_1=469$	$\xi_2=011$	1.4038×10^{-9}	1.3149×10^{-9}	$\pm 0.6598 \times 10^{-9}$	$\pm 0.6545 \times 10^{-9}$
	$\xi_1=337$	$\xi_2=162$	1.5036×10^{-9}	1.4398×10^{-9}			
	$\xi_1=704$	$\xi_2=311$	0.1655×10^{-9}	0.1132×10^{-9}			
	$\xi_1=528$	$\xi_2=165$	0.9186×10^{-9}	0.8735×10^{-9}			
$\mathbf{C}(\mathbf{N}_4 + \mathbf{N}_0(\xi_1))^*$	$\xi_1=196$	$\xi_2=251$	1.2454×10^{-9}	1.2065×10^{-9}			
	$\xi_1=616$	$\xi_2=473$	1.2486×10^{-9}	1.2120×10^{-9}			
	$\xi_1=351$	$\xi_2=830$	1.2402×10^{-9}	1.2018×10^{-9}			
	$\xi_1=585$	$\xi_2=549$	1.2506×10^{-9}	1.2120×10^{-9}			
	$\xi_1=917$	$\xi_2=285$	1.2407×10^{-9}	1.1998×10^{-9}			
	$\xi_1=757$	$\xi_2=753$	1.2537×10^{-9}	1.2153×10^{-9}			
	$\xi_1=380$	$\xi_2=567$	1.2522×10^{-9}	1.2121×10^{-9}			
	$\xi_1=351$	$\xi_2=876$	1.2416×10^{-9}	1.2032×10^{-9}			
	$\xi_1=940$	$\xi_2=551$	1.2504×10^{-9}	1.2107×10^{-9}			
	$\mathbf{C}(\mathbf{N}_4 + \mathbf{N}_0(\xi_1))^*$	$\xi_1=623$	$\xi_2=208$	1.2450×10^{-9}	1.2059×10^{-9}	1.2443×10^{-9}	1.2061×10^{-9}
	$\mathbf{C}(\mathbf{N}_4 + \mathbf{N}_0(\xi_2))^*$	$\xi_1=588$	$\xi_2=302$	1.2532×10^{-9}	1.2164×10^{-9}	$\pm 0.0057 \times 10^{-9}$	$\pm 0.0059 \times 10^{-9}$
	$\xi_1=471$	$\xi_2=845$	1.2483×10^{-9}	1.2096×10^{-9}			
	$\xi_1=231$	$\xi_2=195$	1.2438×10^{-9}	1.2085×10^{-9}			
	$\xi_1=171$	$\xi_2=436$	1.2379×10^{-9}	1.2000×10^{-9}			
	$\xi_1=312$	$\xi_2=431$	1.2323×10^{-9}	1.1918×10^{-9}			
	$\xi_1=924$	$\xi_2=185$	1.2391×10^{-9}	1.2012×10^{-9}			
	$\xi_1=905$	$\xi_2=185$	1.2398×10^{-9}	1.2032×10^{-9}			
	$\xi_1=905$	$\xi_2=439$	1.2386×10^{-9}	1.2019×10^{-9}			
	$\xi_1=980$	$\xi_2=112$	1.2422×10^{-9}	1.2044×10^{-9}			
	$\xi_1=630$	$\xi_2=222$	1.2447×10^{-9}	1.2060×10^{-9}			
$\xi_1=712$	$\xi_2=118$	1.2427×10^{-9}	1.2063×10^{-9}				

TABLE VI. Parameters and results under noises $\mathbf{N}_4 + \mathbf{N}_1(\xi_1)$ and $\mathbf{N}_4 + \mathbf{N}_1(\xi_2)$. Blue data are results with the chosen measurement range of $1.0 \times 10^{-9} < \Theta < 1.6 \times 10^{-9}$.

$\mathbf{N}(t, \xi_1)$	$\mathbf{N}(t, \xi_2)$	Θ_0	Θ_τ
$\xi_1=815$	$\xi_2=127$	1.7590×10^{-9}	1.6588×10^{-9}
$\xi_1=906$	$\xi_2=914$	2.9558×10^{-9}	2.8484×10^{-9}
$\xi_1=633$	$\xi_2=279$	1.3208×10^{-9}	1.2371×10^{-9}
$\xi_1=098$	$\xi_2=547$	2.8010×10^{-9}	2.7208×10^{-9}
$\xi_1=958$	$\xi_2=158$	2.4295×10^{-9}	2.3398×10^{-9}
$\xi_1=995$	$\xi_2=971$	1.6269×10^{-9}	1.5259×10^{-9}
$\xi_1=486$	$\xi_2=142$	1.4278×10^{-9}	1.3268×10^{-9}
$\xi_1=422$	$\xi_2=793$	1.0528×10^{-9}	0.9448×10^{-9}
$\xi_1=565$	$\xi_2=850$	2.0782×10^{-9}	1.9761×10^{-9}
$\xi_1=036$	$\xi_2=934$	2.4629×10^{-9}	2.4073×10^{-9}
$\xi_1=679$	$\xi_2=744$	0.1295×10^{-9}	0.0523×10^{-9}
$\xi_1=172$	$\xi_2=032$	1.8407×10^{-9}	1.7988×10^{-9}
$\xi_1=277$	$\xi_2=098$	0.2199×10^{-9}	0.0941×10^{-9}
$\xi_1=047$	$\xi_2=824$	1.8649×10^{-9}	1.7949×10^{-9}
$\xi_1=439$	$\xi_2=766$	0.5394×10^{-9}	0.4916×10^{-9}
$\xi_1=382$	$\xi_2=796$	0.2860×10^{-9}	0.1662×10^{-9}
$\xi_1=318$	$\xi_2=035$	1.2604×10^{-9}	1.1697×10^{-9}
$\xi_1=187$	$\xi_2=446$	2.3471×10^{-9}	2.2388×10^{-9}
$\xi_1=490$	$\xi_2=647$	0.9874×10^{-9}	0.8682×10^{-9}
$\xi_1=710$	$\xi_2=277$	2.8183×10^{-9}	2.7226×10^{-9}
$\xi_1=755$	$\xi_2=680$	1.3826×10^{-9}	1.3434×10^{-9}
$\xi_1=656$	$\xi_2=119$	1.3386×10^{-9}	1.2747×10^{-9}
$\xi_1=163$	$\xi_2=499$	0.7370×10^{-9}	0.6369×10^{-9}
$\xi_1=960$	$\xi_2=586$	1.3842×10^{-9}	1.3061×10^{-9}
$\xi_1=341$	$\xi_2=244$	1.2322×10^{-9}	1.1610×10^{-9}
$\xi_1=752$	$\xi_2=506$	1.0751×10^{-9}	1.0354×10^{-9}
$\xi_1=256$	$\xi_2=700$	0.9786×10^{-9}	0.9095×10^{-9}
$\xi_1=891$	$\xi_2=548$	0.4792×10^{-9}	0.4259×10^{-9}
$\xi_1=150$	$\xi_2=841$	2.2349×10^{-9}	2.1428×10^{-9}
$\xi_1=258$	$\xi_2=255$	2.3667×10^{-9}	2.2959×10^{-9}
$\xi_1=815$	$\xi_2=930$	0.9187×10^{-9}	0.8185×10^{-9}
$\xi_1=244$	$\xi_2=350$	1.6814×10^{-9}	1.6213×10^{-9}
$\xi_1=197$	$\xi_2=617$	1.9379×10^{-9}	1.8578×10^{-9}
$\xi_1=252$	$\xi_2=474$	2.1893×10^{-9}	2.0974×10^{-9}
$\xi_1=352$	$\xi_2=586$	0.6456×10^{-9}	0.5965×10^{-9}
$\xi_1=918$	$\xi_2=758$	0.5562×10^{-9}	0.4533×10^{-9}
$\xi_1=286$	$\xi_2=754$	1.2889×10^{-9}	1.1970×10^{-9}
$\xi_1=381$	$\xi_2=076$	2.2543×10^{-9}	2.1791×10^{-9}
$\xi_1=586$	$\xi_2=054$	1.0676×10^{-9}	1.0006×10^{-9}
$\xi_1=531$	$\xi_2=935$	0.8742×10^{-9}	0.7992×10^{-9}
$\xi_1=780$	$\xi_2=130$	0.5269×10^{-9}	0.4468×10^{-9}
$\xi_1=569$	$\xi_2=012$	1.1694×10^{-9}	1.1156×10^{-9}
$\xi_1=163$	$\xi_2=312$	0.6913×10^{-9}	0.5912×10^{-9}
$\xi_1=795$	$\xi_2=529$	2.5265×10^{-9}	2.4462×10^{-9}
$\xi_1=166$	$\xi_2=263$	1.3230×10^{-9}	1.2946×10^{-9}

$\mathbf{N}(t, \xi_1)$	$\mathbf{N}(t, \xi_2)$	Θ_0	Θ_τ
$\xi_1=620$	$\xi_2=655$	2.2045×10^{-9}	2.1539×10^{-9}
$\xi_1=690$	$\xi_2=451$	2.1462×10^{-9}	2.1019×10^{-9}
$\xi_1=749$	$\xi_2=084$	1.4580×10^{-9}	1.3755×10^{-9}
$\xi_1=229$	$\xi_2=153$	2.0340×10^{-9}	1.9369×10^{-9}
$\xi_1=539$	$\xi_2=079$	0.8654×10^{-9}	0.7499×10^{-9}
$\xi_1=997$	$\xi_2=443$	2.3088×10^{-9}	2.2146×10^{-9}
$\xi_1=107$	$\xi_2=005$	2.4785×10^{-9}	2.3845×10^{-9}
$\xi_1=962$	$\xi_2=775$	2.1605×10^{-9}	2.2204×10^{-9}
$\xi_1=818$	$\xi_2=085$	2.0225×10^{-9}	1.9191×10^{-9}
$\xi_1=869$	$\xi_2=400$	1.5232×10^{-9}	1.4316×10^{-9}
$\xi_1=360$	$\xi_2=432$	1.2660×10^{-9}	1.1953×10^{-9}
$\xi_1=182$	$\xi_2=146$	0.7204×10^{-9}	0.6624×10^{-9}
$\xi_1=264$	$\xi_2=137$	1.6339×10^{-9}	1.5521×10^{-9}
$\xi_1=870$	$\xi_2=550$	1.7920×10^{-9}	1.7123×10^{-9}
$\xi_1=580$	$\xi_2=145$	1.6182×10^{-9}	1.5089×10^{-9}
$\xi_1=548$	$\xi_2=531$	1.0375×10^{-9}	0.9650×10^{-9}
$\xi_1=420$	$\xi_2=240$	2.0594×10^{-9}	1.9429×10^{-9}
$\xi_1=076$	$\xi_2=124$	1.5390×10^{-9}	1.4767×10^{-9}
$\xi_1=184$	$\xi_2=417$	1.8131×10^{-9}	1.7329×10^{-9}
$\xi_1=240$	$\xi_2=050$	1.2821×10^{-9}	1.1723×10^{-9}
$\xi_1=903$	$\xi_2=491$	1.3023×10^{-9}	1.2327×10^{-9}
$\xi_1=945$	$\xi_2=490$	2.6437×10^{-9}	2.5649×10^{-9}
$\xi_1=338$	$\xi_2=370$	1.1205×10^{-9}	1.0011×10^{-9}
$\xi_1=901$	$\xi_2=112$	1.8895×10^{-9}	1.8216×10^{-9}
$\xi_1=781$	$\xi_2=242$	1.6167×10^{-9}	1.5599×10^{-9}
$\xi_1=097$	$\xi_2=943$	0.7826×10^{-9}	0.6742×10^{-9}
$\xi_1=132$	$\xi_2=967$	2.5019×10^{-9}	2.4104×10^{-9}
$\xi_1=576$	$\xi_2=235$	0.6905×10^{-9}	0.6364×10^{-9}
$\xi_1=060$	$\xi_2=354$	0.0453×10^{-9}	-0.0131×10^{-9}
$\xi_1=822$	$\xi_2=044$	2.1784×10^{-9}	2.1216×10^{-9}
$\xi_1=016$	$\xi_2=169$	1.0362×10^{-9}	0.9469×10^{-9}
$\xi_1=650$	$\xi_2=648$	1.0791×10^{-9}	0.9904×10^{-9}
$\xi_1=549$	$\xi_2=745$	1.1601×10^{-9}	1.0509×10^{-9}
$\xi_1=297$	$\xi_2=179$	1.2751×10^{-9}	1.2043×10^{-9}
$\xi_1=768$	$\xi_2=369$	1.9026×10^{-9}	1.8174×10^{-9}
$\xi_1=184$	$\xi_2=629$	1.9553×10^{-9}	1.8751×10^{-9}
$\xi_1=781$	$\xi_2=930$	0.6486×10^{-9}	0.5919×10^{-9}
$\xi_1=082$	$\xi_2=776$	0.2735×10^{-9}	0.2218×10^{-9}
$\xi_1=480$	$\xi_2=447$	1.0364×10^{-9}	0.9648×10^{-9}
$\xi_1=509$	$\xi_2=818$	0.2596×10^{-9}	0.2201×10^{-9}
$\xi_1=511$	$\xi_2=796$	0.9231×10^{-9}	0.8429×10^{-9}
$\xi_1=645$	$\xi_2=812$	1.2011×10^{-9}	1.0924×10^{-9}
Θ_{Min}	Θ_{Max}	$\bar{\Theta}_0$	$\bar{\Theta}_\tau$
0.0×10^{-9}	3.0×10^{-9}	1.4561×10^{-9}	1.3764×10^{-9}
		$\pm 0.7051 \times 10^{-9}$	$\pm 0.7052 \times 10^{-9}$
1.0×10^{-9}	1.6×10^{-9}	1.2429×10^{-9}	1.1620×10^{-9}
		$\pm 0.1534 \times 10^{-9}$	$\pm 0.1566 \times 10^{-9}$

- [1] K. Pawłowski, D. Spehner, A. Minguzzi, and G. Ferrini, Macroscopic superpositions in bose-josephson junctions: Controlling decoherence due to atom losses, *Phys. Rev. A* **88**, 013606 (2013).
- [2] P. Szańkowski, G. Ramon, J. Krzywda, D. Kwiatkowski, and L. Cywiński, Environmental noise spectroscopy with qubits subjected to dynamical decoupling, *Journal of Physics: Condensed Matter* **29**, 333001 (2017).
- [3] F.-Y. Ma, J.-G. Li, and J. Zou, The influence of non-gaussian noise on weak values, *Physics Letters A* **388**, 127027 (2021).
- [4] M. Abe and M. Ban, Decoherence of a weak value influenced by a non-Markovian environment, *Quantum Studies: Mathematics and Foundations* **3**, 313 (2016).
- [5] M. Ban, Weak measurement on a quantum system in contact with a thermal reservoir: projection operator method, *Quantum Studies: Mathematics and Foundations* **4**, 339 (2017).
- [6] H. Strobel, W. Muessel, D. Linnemann, T. Zibold, D. B. Hume, L. Pezzè, A. Smerzi, and M. K. Oberthaler, Fisher information and entanglement of non-gaussian spin states, *Science* **345**, 424 (2014).
- [7] Q. Guan, G. W. Biedermann, A. Schwettmann, and R. J. Lewis-Swan, Tailored generation of quantum states in an entangled spinor interferometer to overcome detection noise, *Phys. Rev. A* **104**, 042415 (2021).
- [8] A. Rath, C. Branciard, A. Minguzzi, and B. Vermersch, Quantum fisher information from randomized measurements, *Phys. Rev. Lett.* **127**, 260501 (2021).
- [9] B. P. A. et al, Characterization of transient noise in advanced LIGO relevant to gravitational wave signal GW150914, *Classical and Quantum Gravity* **33**, 134001 (2016).
- [10] N. J. Cornish, T. B. Littenberg, B. Bécsy, K. Chatziioannou, J. A. Clark, S. Ghonge, and M. Millhouse, Bayeswave analysis pipeline in the era of gravitational wave observations, *Phys. Rev. D* **103**, 044006 (2021).
- [11] N. J. Cornish and T. B. Littenberg, Bayeswave: Bayesian inference for gravitational wave bursts and instrument glitches, *Classical and Quantum Gravity* **32**, 135012 (2015).
- [12] J. Y. L. Kwok, R. K. L. Lo, A. J. Weinstein, and T. G. F. Li, Investigation of the effects of non-gaussian noise transients and their mitigation in parameterized gravitational-wave tests of general relativity, *Phys. Rev. D* **105**, 024066 (2022).
- [13] B. Zackay, T. Venumadhav, J. Roulet, L. Dai, and M. Zaldarriaga, Detecting gravitational waves in data with non-stationary and non-gaussian noise, *Phys. Rev. D* **104**, 063034 (2021).
- [14] Y. Makhlin, G. Schön, and A. Shnirman, Quantum-state engineering with josephson-junction devices, *Rev. Mod. Phys.* **73**, 357 (2001).
- [15] A. K. Nguyen and S. M. Girvin, Non-gaussian noise in quantum spin glasses and interacting two-level systems, *Phys. Rev. Lett.* **87**, 127205 (2001).
- [16] Y. Aharonov, D. Z. Albert, and L. Vaidman, How the result of a measurement of a component of the spin of a spin-1/2 particle can turn out to be 100, *Phys. Rev. Lett.* **60**, 1351 (1988).
- [17] J. Dressel, M. Malik, F. M. Miatto, A. N. Jordan, and R. W. Boyd, Colloquium: Understanding quantum weak values: Basics and applications, *Rev. Mod. Phys.* **86**, 307 (2014).
- [18] J. Ren, L. Qin, W. Feng, and X.-Q. Li, Weak-value-amplification analysis beyond the aharonov-albert-vaidman limit, *Phys. Rev. A* **102**, 042601 (2020).
- [19] P. Yin, W.-H. Zhang, L. Xu, Z.-G. Liu, W.-F. Zhuang, L. Chen, M. Gong, Y. Ma, X.-X. Peng, G.-C. Li, J.-S. Xu, Z.-Q. Zhou, L. Zhang, G. Chen, C.-F. Li, and G.-C. Guo, Improving the precision of optical metrology by detecting fewer photons with biased weak measurement, *Light: Science & Applications* **10**, 103 (2021).
- [20] F. Lecocq, L. Ranzani, G. A. Peterson, K. Cicak, X. Y. Jin, R. W. Simmonds, J. D. Teufel, and J. Aumentado, Efficient qubit measurement with a nonreciprocal microwave amplifier, *Phys. Rev. Lett.* **126**, 020502 (2021).
- [21] C. Krafczyk, A. N. Jordan, M. E. Goggin, and P. G. Kwiat, Enhanced weak-value amplification via photon recycling, *Phys. Rev. Lett.* **126**, 220801 (2021).
- [22] J. T. Monroe, N. Yunger Halpern, T. Lee, and K. W. Murch, Weak measurement of a superconducting qubit reconciles incompatible operators, *Phys. Rev. Lett.* **126**, 100403 (2021).
- [23] G. I. Viza, J. Martínez-Rincón, G. A. Howland, H. Frostig, I. Shomroni, B. Dayan, and J. C. Howell, Weak-values technique for velocity measurements, *Opt. Lett.* **38**, 2949 (2013).
- [24] J.-H. Huang, F.-F. He, X.-Y. Duan, G.-J. Wang, and X.-Y. Hu, Modified weak-value-amplification technique for measuring a mirror's velocity based on the vernier effect, *Phys. Rev. A* **105**, 013718 (2022).
- [25] B. de Lima Bernardo, S. Azevedo, and A. Rosas, Ultra-small polarization rotation measurements via weak value amplification, *Physics Letters A* **378**, 2029 (2014).
- [26] O. S. Magaña Loaiza, M. Mirhosseini, B. Rodenburg, and R. W. Boyd, Amplification of angular rotations using weak measurements, *Phys. Rev. Lett.* **112**, 200401 (2014).
- [27] X.-Y. Xu, Y. Kedem, K. Sun, L. Vaidman, C.-F. Li, and G.-C. Guo, Phase estimation with weak measurement using a white light source, *Phys. Rev. Lett.* **111**, 033604 (2013).
- [28] Y. Yang, Y. Xu, T. Guan, L. Shi, J. Li, D. Li, Y. He, X. Wang, Z. Li, and Y. Ji, Spectrum intensity ratio detection for frequency domain weak measurement system, *IEEE Photonics Journal* **12**, 1 (2020).
- [29] J.-H. Huang, X.-Y. Duan, G.-J. Wang, and X.-Y. Hu, Enhancing the precision of detecting weak magnetic fields based on weak-value amplification, *J. Opt. Soc. Am. B* **39**, 1289 (2022).
- [30] D. J. Starling, P. B. Dixon, A. N. Jordan, and J. C. Howell, Optimizing the signal-to-noise ratio of a beam-deflection measurement with interferometric weak values, *Phys. Rev. A* **80**, 041803 (2009).
- [31] N. Modak, A. B S, A. K. Singh, and N. Ghosh, Generalized framework of weak-value amplification in path interference of polarized light for the enhancement of all possible polarization anisotropy effects, *Phys. Rev. A* **103**, 053518 (2021).
- [32] J. Harris, R. W. Boyd, and J. S. Lundeen, Weak value amplification can outperform conventional measurement

- in the presence of detector saturation, *Phys. Rev. Lett.* **118**, 070802 (2017).
- [33] J. Martínez-Rincón, W.-T. Liu, G. I. Viza, and J. C. Howell, Can anomalous amplification be attained without postselection?, *Phys. Rev. Lett.* **116**, 100803 (2016).
- [34] M. Song, J. Steinmetz, Y. Zhang, J. Nauriyal, K. Lyons, A. N. Jordan, and J. Cardenas, Enhanced on-chip phase measurement by inverse weak value amplification, *Nat. Commun.* **12**, 6247 (2021).
- [35] Y. Kim, S.-Y. Yoo, and Y.-H. Kim, Heisenberg-limited metrology via weak-value amplification without using entangled resources, *Phys. Rev. Lett.* **128**, 040503 (2022).
- [36] Y. Wang, W. Zhang, S. Chen, S. Wen, and H. Luo, Multiple-weak-value quantum measurement for precision estimation of time delay, *Phys. Rev. A* **105**, 033521 (2022).
- [37] Z.-P. Li, Y.-T. Wang, S. Yu, W. Liu, Y. Meng, Y.-Z. Yang, Z.-A. Wang, N.-J. Guo, X.-D. Zeng, J.-S. Tang, C.-F. Li, and G.-C. Guo, Experimental investigation of high-efficiency weak-value amplification of nonunitary evolution, *Phys. Rev. A* **106**, 012608 (2022).
- [38] A. Nishizawa, K. Nakamura, and M.-K. Fujimoto, Weak-value amplification in a shot-noise-limited interferometer, *Phys. Rev. A* **85**, 062108 (2012).
- [39] J. Sinclair, M. Hallaji, A. M. Steinberg, J. Tollaksen, and A. N. Jordan, Weak-value amplification and optimal parameter estimation in the presence of correlated noise, *Phys. Rev. A* **96**, 052128 (2017).
- [40] X. Zhu and Y.-X. Zhang, Influence of environmental noise on the weak value amplification, *Quantum Information Processing* **15**, 3421 (2016).
- [41] H. Wu, P. Wu, Z.-C. Luo, L.-P. Xu, J.-H. Xie, T.-Y. Chang, H.-F. Shi, C.-L. Du, and H.-L. Cui, Pragmatic implementation with non-gaussian devices of noise-limited weak value amplification, *IEEE Photonics Journal* **13**, 1 (2021).
- [42] H. Wu, Z.-C. Luo, L.-P. Xu, P. Wu, H.-F. Shi, T.-Y. Chang, C.-L. Du, Y. Liu, Y.-G. Lu, and H.-L. Cui, Effects of nonlinearity and technical noise on weak-value amplified phase measurement, *Journal of Physics B: Atomic, Molecular and Optical Physics* **53**, 125401 (2020).
- [43] J.-H. Huang, X.-Y. Hu, A. Dada, J. S. Lundeen, K. M. Jordan, H. Chen, and J.-Q. An, Auto-correlative weak-value amplification under strong noise background, *arXiv* **104**, 063034 (2021).
- [44] R. F. Fox, I. R. Gatland, R. Roy, and G. Vemuri, Fast, accurate algorithm for numerical simulation of exponentially correlated colored noise, *Phys. Rev. A* **38**, 5938 (1988).
- [45] B. L. Hu, J. P. Paz, and Y. Zhang, Quantum brownian motion in a general environment: Exact master equation with nonlocal dissipation and colored noise, *Phys. Rev. D* **45**, 2843 (1992).
- [46] J.-L. Wu, W.-L. Duan, Y. Luo, and F. Yang, Time delay and non-gaussian noise-enhanced stability of foraging colony system, *Phys. A* **553**, 124253 (2020).
- [47] O. V. Pountougnigni, R. Yamapi, C. Tchawoua, V. Pierro, and G. Filatrella, Detection of signals in presence of noise through josephson junction switching currents, *Phys. Rev. E* **101**, 052205 (2020).
- [48] R. Jozsa, Complex weak values in quantum measurement, *Phys. Rev. A* **76**, 044103 (2007).
- [49] Y. Susa, Y. Shikano, and A. Hosoya, Optimal probe wave function of weak-value amplification, *Phys. Rev. A* **85**, 052110 (2012).
- [50] Y. Shikano and A. Hosoya, Weak values with decoherence, *J. Phys. A: Math. Theor.* **43**, 025304 (2009).
- [51] M. Abe and M. Ban, Decoherence of weak values in a pure dephasing process, *Quantum Studies: Mathematics and Foundations* **2**, 23 (2015).
- [52] Y. Lee, T. Cheatham, and J. Wiesner, Application of correlation analysis to the detection of periodic signals in noise, *Proc. IRE* **38**, 1165 (1950).
- [53] Y. Liu, J. Liu, and R. Kennel, Frequency measurement method of signals with low signal-to-noise-ratio using cross-correlation, *Machines* **9**, 10.3390/machines9060123 (2021).
- [54] E. J. Takahashi, P. Lan, O. D. Mücke, Y. Nabekawa, and K. Midorikawa, Attosecond nonlinear optics using gigawatt-scale isolated attosecond pulses, *Nat. Commun.* **4**, 2691 (2013).
- [55] G. C. Knee and E. M. Gauger, When amplification with weak values fails to suppress technical noise, *Phys. Rev. X* **4**, 011032 (2014).
- [56] C. Ferrie and J. Combes, Weak value amplification is suboptimal for estimation and detection, *Phys. Rev. Lett.* **112**, 040406 (2014).
- [57] V. Galdi, V. Pierro, and I. M. Pinto, Evaluation of stochastic-resonance-based detectors of weak harmonic signals in additive white gaussian noise, *Phys. Rev. E* **57**, 6470 (1998).
- [58] E. Thrane and C. Talbot, An introduction to bayesian inference in gravitational-wave astronomy: Parameter estimation, model selection, and hierarchical models, *Publications of the Astronomical Society of Australia* **36**, e010 (2019).
- [59] H. Wong, Low-frequency noise study in electron devices: review and update, *Microelectronics Reliability* **43**, 585 (2003).
- [60] S. V. Vaseghi, *Advanced Digital Signal Processing and Noise Reduction* (John Wiley and Sons, Ltd, 2005).
- [61] T. L. Floyd, *Digital Fundamentals (10th Edition)* (Prentice Hall, 2008).
- [62] S. Mondal, P. Ray, and J. Maiti, Modelling robustness for manufacturing processes: a critical review, *Int. J. Prod. Res.* **52**, 521 (2014), <https://doi.org/10.1080/00207543.2013.837588>.
- [63] S. Zhong, J. Xu, and X. Zhou, High-efficiency zero-voltage switching single-stage switching amplifier with half-bridge active clamping circuit, *IRE Trans. Ind. Electron.* **65**, 8574 (2018).
- [64] F. Peters, A. Gennerich, D. Czesnik, and D. Schild, Low frequency voltage clamp: recording of voltage transients at constant average command voltage, *J. Neurosci. Methods* **99**, 129 (2000).
- [65] J. Schröder, M. A. F. Roelens, L. B. Du, A. J. Lowery, S. Frisken, and B. J. Eggleton, An optical fpga: Reconfigurable simultaneous multi-output spectral pulse-shaping for linear optical processing, *Opt. Express* **21**, 690 (2013).
- [66] X. Lu, L. Zhang, Y. Wang, W. Chen, D. Huang, D. Li, S. Wang, D. He, Z. Yin, Y. Zhou, C. Hui, and Z. Han, FPGA based digital phase-coding quantum key distribution system, *Sci. China: Phys., Mech. Astron.* **58**, 120301 (2015).
- [67] J. Elaskar, M. A. Luda, L. Tozzetti, J. Codnia, and C. J. Oton, Fpga-based high-speed optical fiber sensor based on multitone-mixing interferometry, *IEEE Trans. Instrum. Meas.* **71**, 1 (2022).